AFRL-IF-RS-TR-2002-190
Final Technical Report
August 2002

EFFICIENT COMPUTATIONAL PROTOTYPING OF MIXED TECHNOLOGY MICROFLUIDIC COMPONENTS AND SYSTEMS

University of Illinois

Sponsored by
Defense Advanced Research Projects Agency
DARPA Order No. G220/12

AIR FORCE RESEARCH LABORATORY
INFORMATION DIRECTORATE
ROME RESEARCH SITE
ROME, NEW YORK

This report has been reviewed by the Air Force Research Laboratory, Information Directorate, Public Affairs Office (IFOIPA) and is releasable to the National Technical Information Service (NTIS). At NTIS it will be releasable to the general public, including foreign nations.

AFRL-IF-RS-TR-2002-190 has been reviewed and is approved for publication

APPROVED: 

GEORGE O. RAMSEYER
Project Engineer

FOR THE DIRECTOR:

MICHAEL L. TALBERT, Technical Advisor
Information Technology Division
Information Directorate

REPORT DOCUMENTATION PAGE

Form Approved
OMB No. 074-0188

1. AGENCY USE ONLY (Leave blank)	2. REPORT DATE	3. REPORT TYPE AND DATES COVERED
	AUGUST 2002	Final May 98 – Sep 01

4. TITLE AND SUBTITLE
EFFICIENT COMPUTATIONAL PROTOTYPING OF MIXED TECHNOLOGY MICROFLUIDIC COMPONENTS AND SYSTEMS

5. FUNDING NUMBERS
C - F30602-98-2-0178
PE - 63739E
PR - E117
TA - 00
WU - 38

6. AUTHOR(S)
Narayan R. Aluru, Jacob White, George E. Kamiadakis, Kartikeya Mayaram, Chang Liu, Juan Santiago, and William Trimmer

7. PERFORMING ORGANIZATION NAME(S) AND ADDRESS(ES)
University of Illinois
109 Coble Hall
801 South Wright Street
Champaign Illinois 61820

8. PERFORMING ORGANIZATION REPORT NUMBER
N/A

9. SPONSORING / MONITORING AGENCY NAME(S) AND ADDRESS(ES)
Defense Advanced Research Projects Agency
3701 North Fairfax Drive
Arlington Virginia 22203-1714

AFRL/IFTC
26 Electronic Parkway
Rome New York 13441-4514

10. SPONSORING / MONITORING AGENCY REPORT NUMBER
AFRL-IF-RS-TR-2002-190

11. SUPPLEMENTARY NOTES
AFRL Project Engineer: George O. Ramseyer/IFTC/(315) 330-3492

12a. DISTRIBUTION / AVAILABILITY STATEMENT
APPROVED FOR PUBLIC RELEASE; DISTRIBUTION UNLIMITED.

12b. DISTRIBUTION CODE

13. ABSTRACT ***(Maximum 200 Words)***
Fast and efficient Computer Aided Design (CAD) tools for microfluidic components and systems were developed in this effort. Innovative numerical methods and algorithms for mixed-technology simulation of microfluidic devices and systems are described. Algorithms and techniques for coupled circuit/device modeling of microfluidic systems are presented. Test structures and devices were fabricated, and measurements taken to enable the computational prototyping of microfluidics and Micro-Electro Mechanical Systems (MEMS).

14. SUBJECT TERMS
Computer Aided Design, CAD, Micro-Electro Mechanical Systems, MEMS, Mixed Technology Simulation, Microfluidic Device, Microfluidic System, Coupled Circuit/Device, Microfluidic Simulation, Microfluidic Modeling

15. NUMBER OF PAGES
59

16. PRICE CODE

17. SECURITY CLASSIFICATION OF REPORT	18. SECURITY CLASSIFICATION OF THIS PAGE	19. SECURITY CLASSIFICATION OF ABSTRACT	20. LIMITATION OF ABSTRACT
UNCLASSIFIED	UNCLASSIFIED	UNCLASSIFIED	UL

TABLE OF CONTENTS

LIST OF FIGURES

LIST OF TABLES

ACKNOWLEDGMENTS

The Principal Investigators would like to thank Dr. Anantha Krishnan, Dr. George Ramseyer, Mr. Clare Thiem and Dr. Heather Dussault for useful suggestions.

1. SUMMARY

The major breakthroughs obtained in the development of the Composite Computer Aided Design (CAD) tools (1) for mixed technology integration in this effort include the developments of:

- FASTSTOKES, which is up to 3 orders of magnitude faster than conventional numerical methods of determining drag forces on geometrically complicated 3-dimensional structures.
- Νεκταr code for analysis of microflows. Νεκταr code includes slip models for smooth as well as rough walls.
- Force coupled method for bioparticulate flows as well as techniques and codes for stochastic modeling of microflows.
- Molecular codes based on Direct Simulation Monte Carlo (DSMC) and molecular dynamics techniques for micro and nanoscale analysis of gas and liquid flows.
- Finite cloud and boundary cloud meshless methods for efficient interior and exterior analysis of microfluidics and MEMS.
- Multiscale methods combining meshless and continuum based microfluidic simulation tools with DSMC. Investigated fundamental physical phenomena in microfilters using multiscale simulation tools.
- New reduced-order models based on weighted Karhunen-Loeve decomposition technique for fast dynamic analysis of microfluidics.
- A framework for coupling SPICE3 with fluidic solvers Νεκταr and EOFLOW. Implemented efficient time stepping schemes for coupled circuit and microfluidic device simulation.

Applications of this software have resulted in the efficient computational prototyping of mixed-technology microfluidic components and systems in:

- Microfabrication and packaging technologies for microfluidic systems based on silicon, glass, elastomer, biodegradable, and liquid crystal polymer materials.
- Demonstrated a micromachined elastomer micropump for remote wireless operation and a magnetic micro bar mixer for mixing fluids in channels and reaction chambers.
- Design rules for the optimization of 90º and 180º constant radius turns in electrophoretic systems. A novel experimental technique, bleached fluorescence visualization, was implemented to verify these predictions.
- Optimized turn geometry, shown to reduce the dispersion variance to less than 1% for a simple turn, was proposed.
- Design of several complex fluidic devices with the developed design software. Several fabrication cycles have been eliminated because of the use of these design tools.
- Initial transition of design tools developed as part of this project to commercial MEMS CAD companies.

2. INTRODUCTION

The objective of this effort titled "Efficient Computational Prototyping of Mixed-Technology Microfluidic Components and Systems" included developing fast and efficient computer-aided design tools for microfluidic components and systems. Innovation in numerical methods and algorithms is critical as we work towards the development of advanced CAD tools for mixed-technology microfluidic devices and systems.

To accomplish this, algorithms and techniques for coupled-domain simulation of mixed-technology MicroElectro Mechanical Systems have been developed. In particular, algorithms and techniques for coupled circuit/device modeling of microfluidic systems have been developed and tested. Test structures and devices were fabricated to verify our models, and measurements were made on the fabricated devices to enable computational prototyping of MEMS. This technology was then transferred to the commercial, university and government researchers.

3. MICROFLUIDIC SIMULATION TOOLS

Three approaches were used to develop microfluidic simulation tools for microfluidic energy domains. FASTSTOKES focuses on fast exterior analysis of microfluidic energy domains. Also, highly accurate spectral methods for analysis were also developed. Thirdly, new computational methods for radically simpler analysis of microfluidic energy domain were explored. Summaries of this work are presented here, and additional details can be found in references 1-18.

3.1 FASTSTOKES

FASTSTOKES is a precorrected-Fast Fourier Transform (FFT) accelerated fluid analysis program for the analysis of the Stokes equation that is as much as three orders of magnitude faster to run than existing finite-element and boundary-element methods when used to analyze complicated micromachined structures. FASTSTOKES is the only fluid analysis program capable of analyzing entire complicated three-dimensional designs. Developing a robust numerical engine and extending the analysis capabilities led to a large number of algorithmic and physical developments.

3.1.1 Basic Solver Technology

Several new algorithms and a new software platform were developed and demonstrated for the precorrected-FFT solver. The algorithmic innovations included a new polynomial projection/interpolation algorithm and a new approach to vector convolution that accelerated the code by nearly a factor of three.

One of the improvements made to FASTSTOKES was to reduce the number of convolutions required to compute grid velocities, given grid forces. In the classical approach (Figure 1), the grid velocities were computed from grid forces using 9 convolutions (a total of 18 Fast Fourier Transforms (FFT's)). The improved FASTSTOKES approach (Figure 2) required only 6 FFT's.

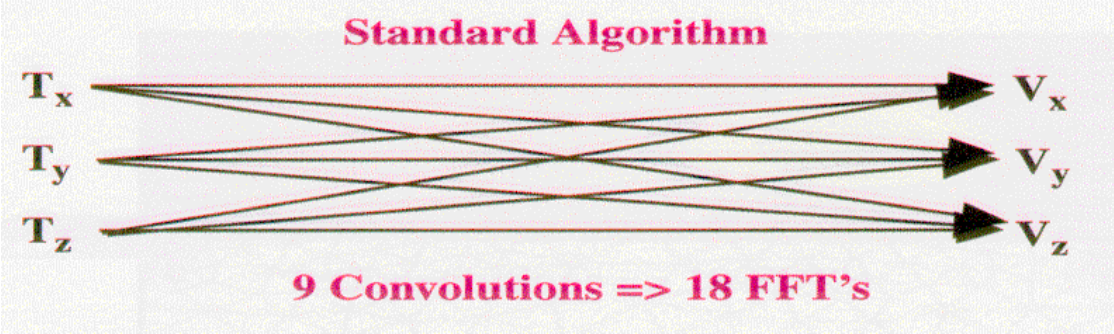

Figure 1. Classical approach to computing grid velocities

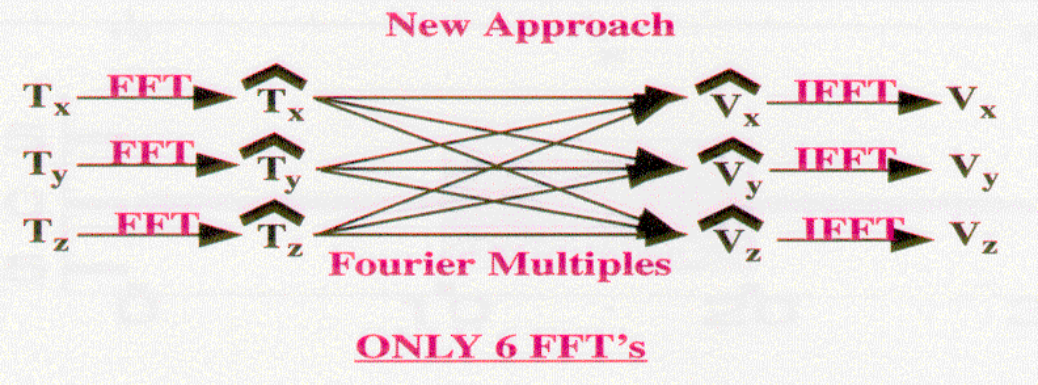

Figure 2. FASTSTOKES approach to computing grid velocities

The first Greens function independent fast solver was developed and demonstrated, which makes use of sparse matrix data structures to make it easy to adapt the code to other applications. The code has been used for applications as diverse as electromagnetic interconnect analysis and offshore structure analysis (FASTWAMIT), as well as for Stokes flow analysis.

Also, the first approach to computing integrals over curved panels was demonstrated that is both accurate and also independent of panel separation distance. The technique used a novel implicit mapping scheme to map the curved surface to a flat one, a recursive algorithm for integrating singularities over flat surfaces, and a specialized quadrature algorithm.

3.1.2 Innovations in FASTSTOKES Flow Analysis

The integral equations for Stokes flow have a well-known singularity for single body problems. Because the codes were too time consuming and computer intensive to use on multiple body problems, the multidimensional singularity for multiple bodies had not been previously examined. An approach to eliminating the singularity and computing the correct drag force distributions by using a combination of a singular-subspace orthogonalized Krylov subspace algorithm and an auxiliary integral pressure boundary condition was developed.

3.1.3 Application of FASTSTOKES to Comb Drive Analysis

The FASTSTOKES Solver was used to compute the drag on comb drives (Figure 3), and the results were correlated with the measured data from Professor Dennis Freeman's (MIT) visualization system for MEMS. The detailed drag force analysis can only be made by using FASTSTOKES, as the drag can not be directly visualized, and showed that only half the drag force on a comb drive is due to comb-substrate interactions. This overturned many commonly accepted analyses in the literature.

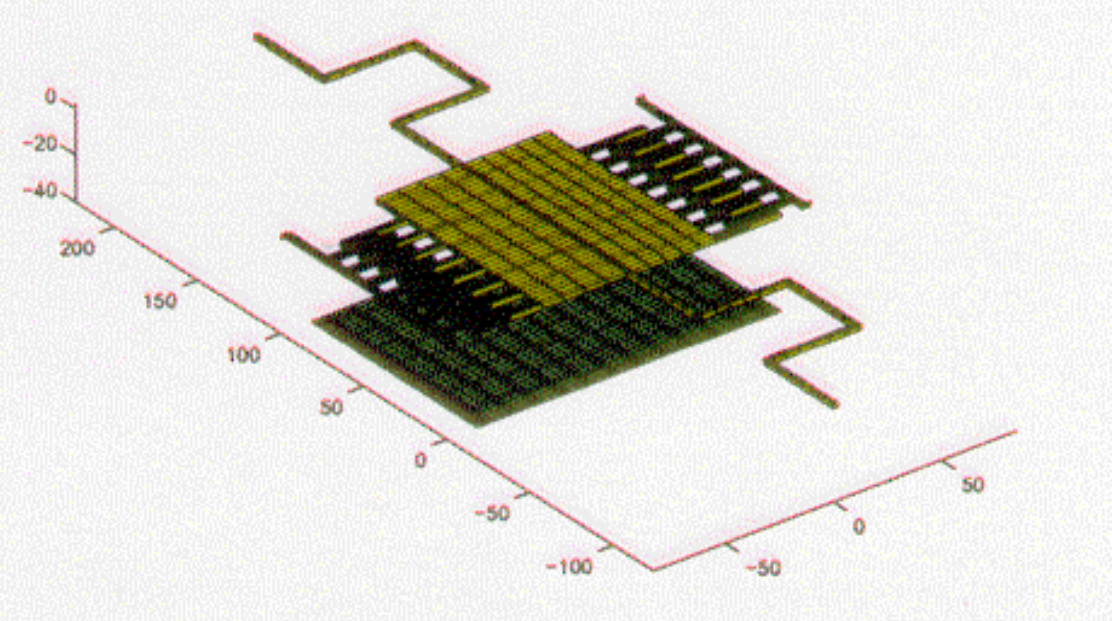

Figure 3. A comb resonator (dimensions in microns)

3.1.4 Extensions of FASTSTOKES to the Unsteady and Compressible Case

The FASTSTOKES code was extended to analyzing both unsteady and mildly compressible Stokes flow. Several new techniques were developed for computing integrals of the frequency-dependent Greens function for the unsteady case. A new linearization approach was developed that can analyze compression without volume discretization for the compressible case. The latter result made it possible to analyze the vertical motion in micromachined devices, which introduces compression, nearly as fast as the analysis of lateral motion, where there is no compression.

3.2 SPECTRAL METHODS

Very efficient spectral/hp methods for analysis of Stokes and Navier-Stokes equations were developed. The spectral/hp methods incorporate both multi-domain spectral methods and high-order finite element methods. Νεκταr, a spectral/hp element code, was developed for microflow analysis. Specific accomplishments in this area included the development of:

- Triangular/Tetrahedral Spectral Elements
- Slip models when rough walls are present in microfluidic devices.
- A force coupled method for bioparticulate (2) flows.
- Techniques and codes for stochastic modeling of microflows.
- Molecular codes for analysis of microflows.

3.2.1 Νεκταr

Νεκταr is a general purpose Computational Fluid Dynamics (CFD) code for simulating incompressible, compressible and plasma flows in unsteady three-dimensional geometries. The code uses meshes similar to standard finite element and finite volume meshes, consisting of structured or unstructured grids or a combination of both. The formulation is also similar to those methods corresponding to Galerkin and discontinuous Galerkin (3) projections for the incompressible and compressible Navier-Stokes equations.

.

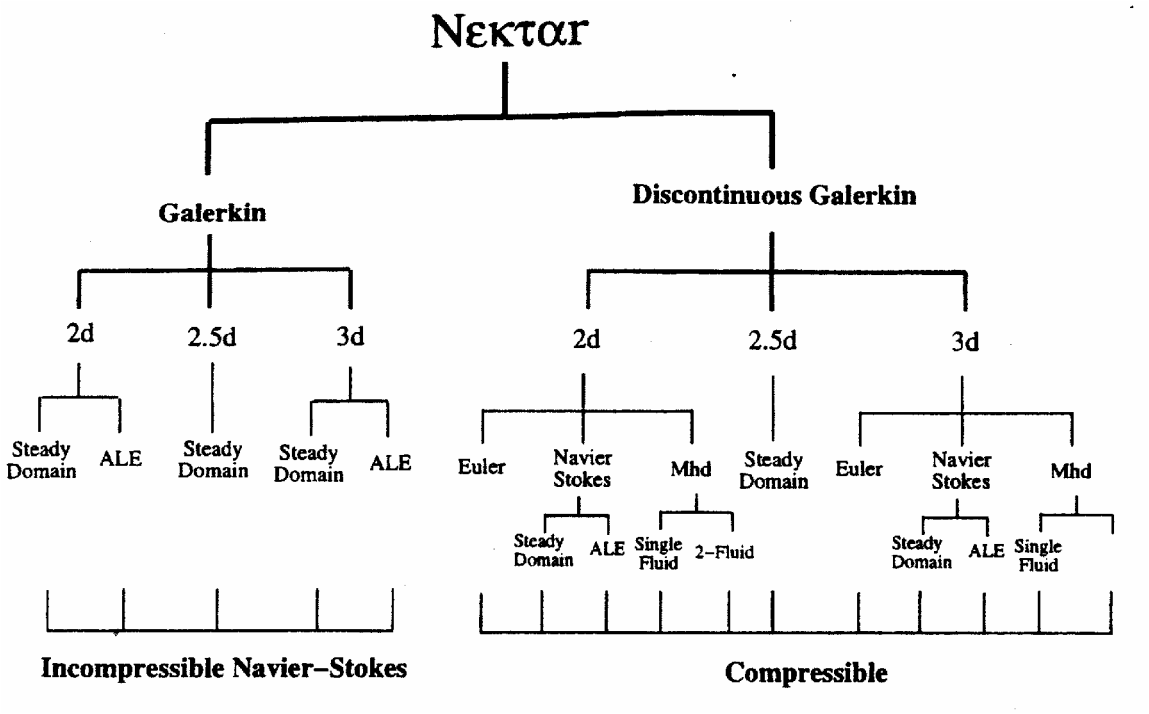

Figure 4. Hierarchy of the Νεκταr code for transient nonlinear flow analysis

In Figure 4 is presented the hierarchy of the Νεκταr code for transient nonlinear flow analysis (4,5). The "2d" and "3d" refers to two-dimensions and three-dimensions, respectively. "2.5d" refers to a three-dimensional capability but with one of the geometric directions being homogeneous in geometry. "ALE" refers to moving computational domains required in dynamic flow-structure interactions. Gaseous microflows can be simulated by either the compressible or incompressible version depending upon the pressure/density variations.

Sets of numerical simulations of dispersed two-phase flow at low to moderate Reynolds numbers for both unbounded domains and ducts with complex geometry have been performed. The code Νεκταr has been employed, with the 3D fluid motion fully resolved by the spectral/hp element method and the coupled momentum and energy between the particle and fluid phases solved by finite-valued force coupling method.

This included both force monopole and dipole terms together with inter-particle and particle-wall collision barriers.

Software tools for post-processing and visualization of data were implemented in MATLAB. This allowed the verification of the results for solid, fluid and circuit elements of Microsystems. As an example of an analysis using Νεκταr, flow in a two-dimensional microfluidics channel has been modeled. As shown in Figure 5, the two ends of the channel are 10 microns long and 1 micron wide. The middle channel is 10 microns long and 10 microns wide. The fluid in the middle channel obeyed continuum theories, and deviations from classical continuum theories was observed in the two thin channels.

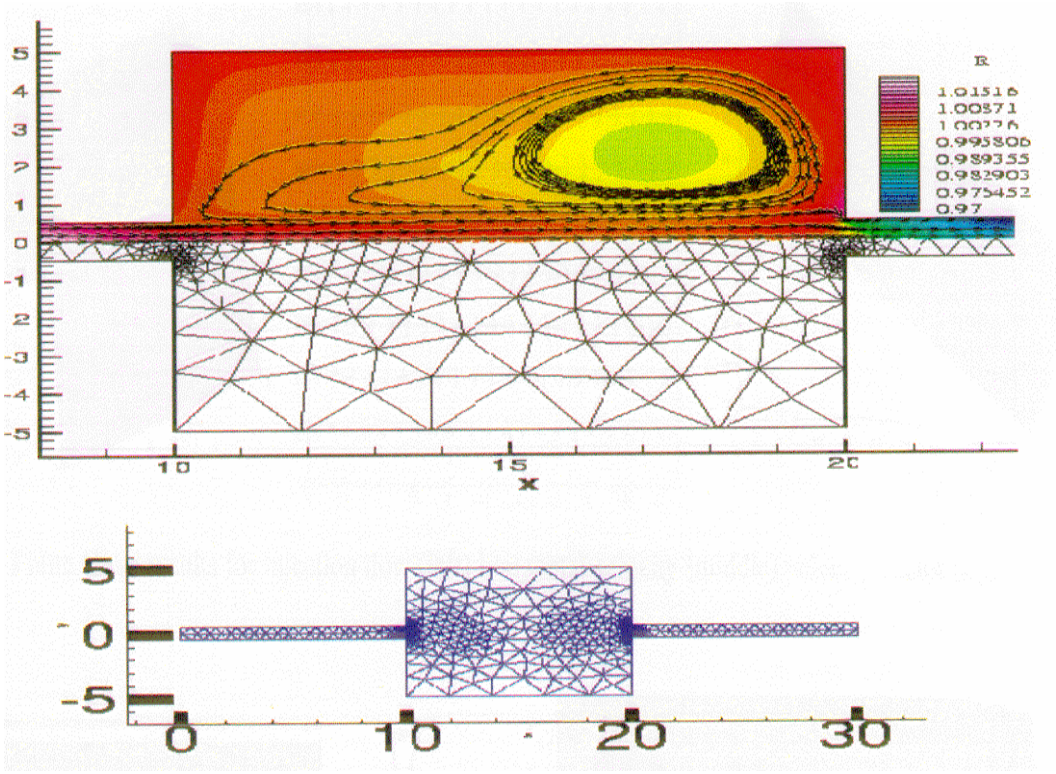

Figure 5. Two-dimensional microflow modeled by Νεκταr

3.2.2 Low-Dimensional Vorticity-Based Models

On the physics side, out objective was to construct low-dimensional, vorticity-based dynamical models for prototype flow-structures interaction problems, based on the simulation databases and supplementary experimental information. In addition, a more fundamental goal was to provide insight to a selected class of these flows and explain such generic phenomena as: Large-scale instabilities of non-stationary turbulent flows (e.g. wakes); flow pattern selection in flow-structure interaction problems; and vorticity generation in free surface flows.

3.3 NEW ALGORITHMS

Several new algorithms were developed, including microfluidic meshless techniques, the boundary cloud method, and reduced order models for fast dynamic analysis of microfluidics. Other new algorithms included a microflow model for the molecular analysis of microfluidic devices and multiscale methods for efficient analysis of microfluidic devices.

The new generation of spectral/hp methods utilizes unstructured meshes, consisting of a mix of triangles/quadrilaterals in two-dimensions or tetrahedra/pyramids/hexahedra in three-dimensions, allowed for efficient dynamic re-discretization "on-the-fly" without the frequent need for costly re-meshing. An initial mesh macro-skeleton consisting of many subdomains can remain unaltered while spectral (p-type) refinement takes place to accommodate new features in the solution. It is only when very large deformations occur that new subdomains need to be introduced, and given the unstructured character of the discretization, this h--type refinement can be local only, preventing global propagation which will greatly disrupt load balancing.

3.3.1 Microfluidic Meshless Techniques

Meshless techniques were developed for the efficient analysis of microfluidics and MEMS applications when microfluidics is one of the energy domains. The routine method of making a mesh for a simulation can be time consuming, particularly when the geometry of the object to be modeled is complex.

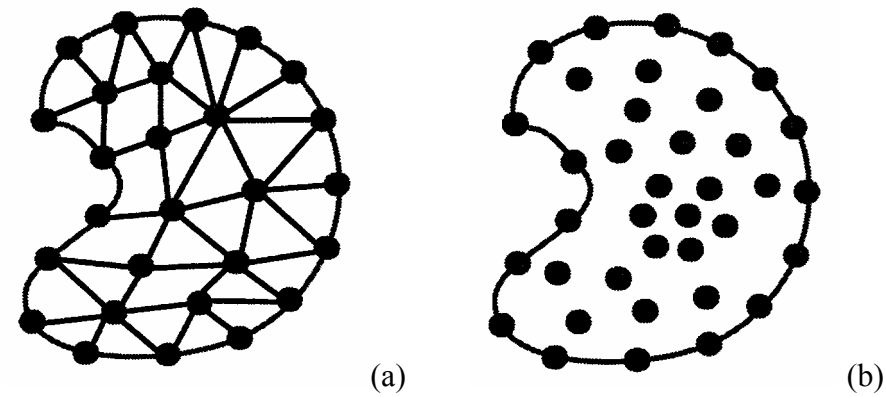

Figure 6. Mesh (a) and meshless (b) approaches

Meshless meshes are a radically simpler approach to MEMS modeling and design. Meshing requirements are very complemented for multiphysics or coupled energy domains, where the meshing demands are very acute. The existing approach of using a mesh requires discretization of the domains and element structure (Figure 6a). With

MEMS modeling, there are moving boundary and structure problems. An alternate method is to use a mesh free approach. This new meshless approach requires only points (6) or particles, and there is no connectivity between the particles (Figure 6b). The meshless approach will result in highly accurate solutions based upon adaptivity and error estimation, and is highly efficient to implement on parallel computers.

3.3.1.1 Finite Point Method

A cross channel is one of the fundamental geometries considered for the lab-on-a-chip concept. The electroosmotic fluidic transport (7) though a cross-channel was simulated using a meshless code based on a weighted least square interpolation is presented for the simulation of electroosmotic transport in capillaries. The geometry of the cross-channel is shown in Figure 7. The point distribution employed for the cross-channel and the velocity vector plot are presented in Figures 8 and 9, respectively.

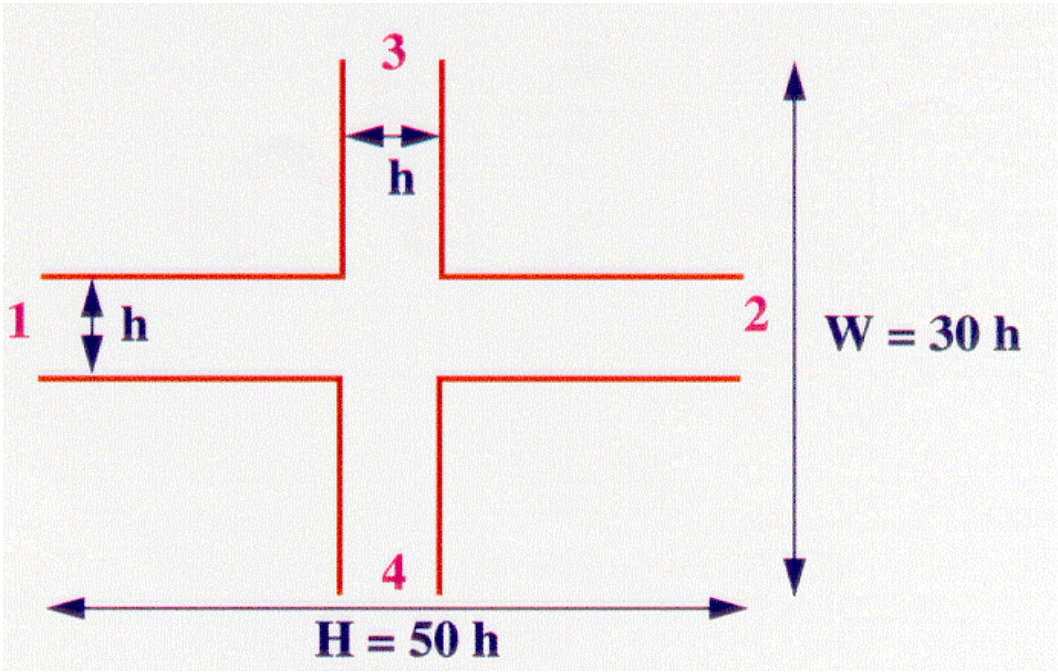

Figure 7. The geometry of the cross-channel

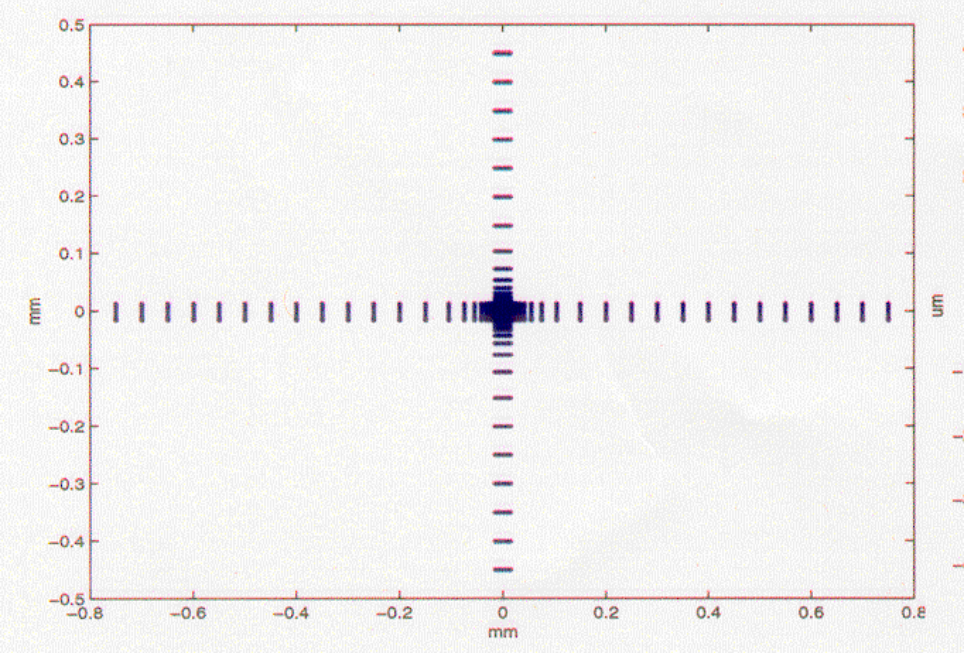

Figure 8. The point distribution for the cross-channel

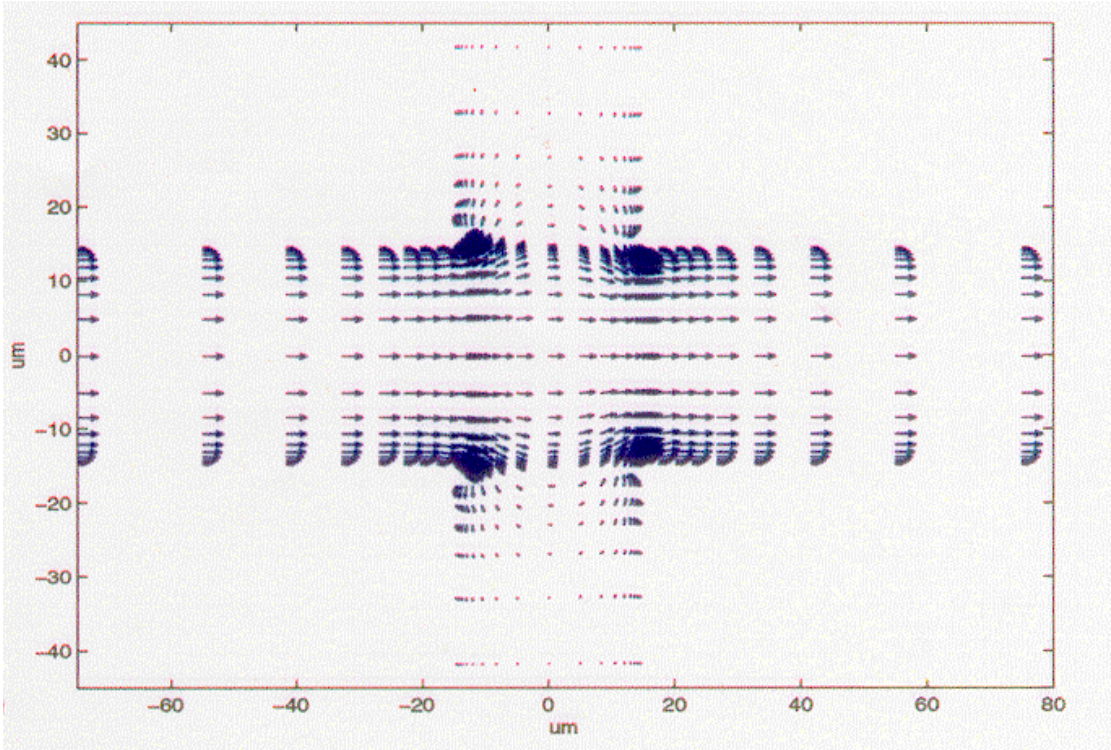

Figure 9. The resultant velocity vectors for symmetric applied potential for the cross-channel

These results matched analytical results published previously for a cross-shaped channel. The advantage of this method over other PDE solvers is the computational savings due to a lack of mesh generation and integration.

3.3.1.2 Finite Cloud Method

A finite cloud method was developed based upon the meshless approach, which was based on a fixed-kernel technique (8) for construction of interpolation functions and a collocation technique for discretization of the Stokes and Navier-Stokes equations. The finite cloud (9) method uses a point distribution, and constructs interpolation functions without assuming any connectivity between the points. A collocation approach is employed to obtain a solution at every point within the domain.

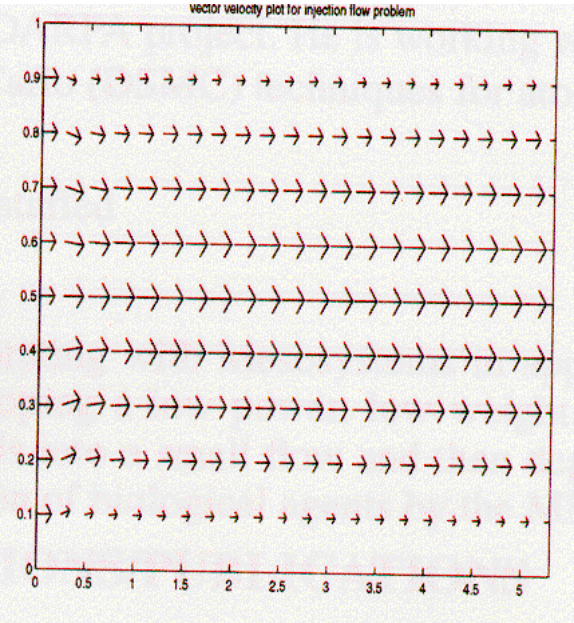

Figure 10. Finite cloud injection flow velocity vectors

The finite cloud method was applied to the analysis of several microfluidic devices, resulting in radically simpler analysis. For example, in Figure 10 is presented the results of the injection velocity vectors determined using the meshless finite cloud method. In Figure 11 are presented the finite cloud method results of the horizontal velocity (a) and the corresponding pressure drop (b) for this same injection flow.

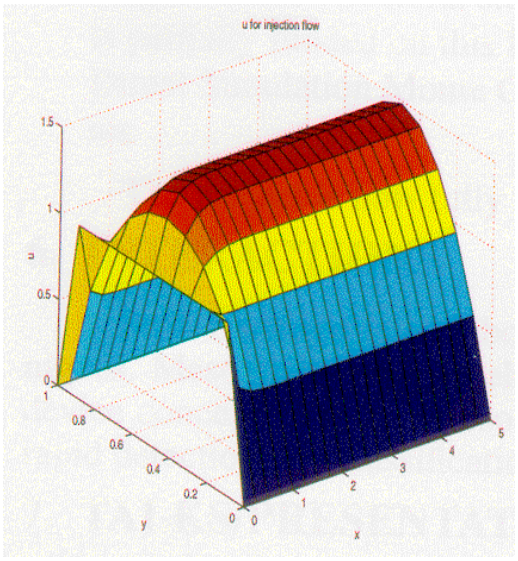

(a)

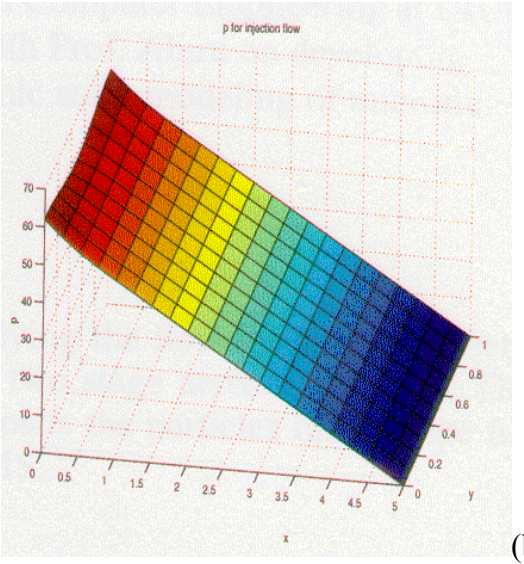

(b)

Figure 11. Finite cloud results for horizontal velocity (a) and pressure drop (b) for an injection flow

In Figure 12 is presented another application of the finite cloud method. In this case a piezoelectric device was modeled (10). The governing equations for the piezoelectric devices were coupled electrical and mechanical equations, and the results obtained were for the application of 1000 V on the electrodes. The piezoelectric material was polarized in the vertical direction, and the vertical axial stresses are displayed in the figure.

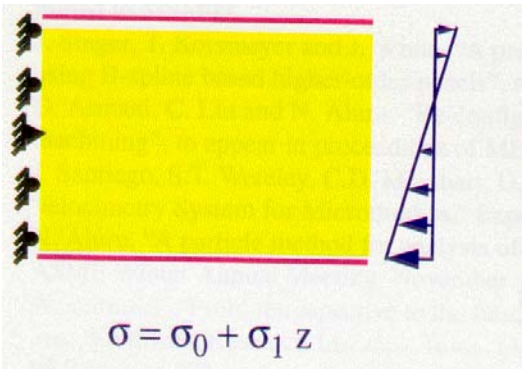

(a)

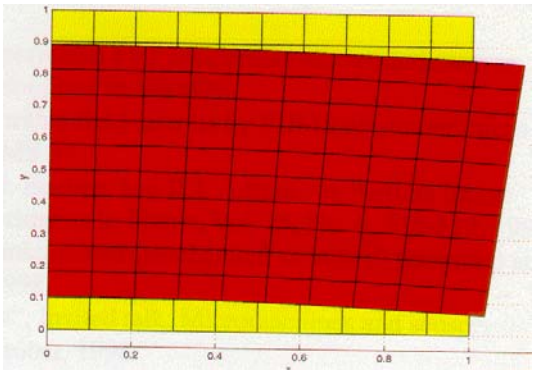

(b)

Figure 12. Finite cloud results for the vertical direction of a piezoelectric device before polarization (a) and after polarization (b) for an applied bias of 1000 volts

3.3.1.3 Boundary Cloud Method

A boundary cloud method is a combined scattered point/boundary integral approach for the boundary only analysis of exterior problems (11). The boundary cloud method has been combined with a singular value decomposition based on fast algorithm for the rapid solution of the linear system. This fast boundary cloud method (12) can be used for rapid analysis of electrostatic (13) and Stokes equations. It was demonstrated the analysis of electrostatic equations.

3.3.2 Reduced-Order Models for Fast Dynamic Analysis of Microfluidics

A new reduced-order model for fast dynamic analysis of microfluidics was developed, based upon a weighted Karhunen-Loeve decomposition approach for efficient and accurate dynamic analysis of electro-osmotic flows. The new approach requires much fewer number of modes compared to the classical reduced-order models, and dramatically reduced the central processor unit (cpu) time required to design highly complex microfluidic devices.

3.3.3 Microflow Model for the Molecular Analysis of Microfluidic Devices

A new microflow model for the molecular analysis of microfluidic devices was developed. This microflow model used the Direct Simulation Monte Carlo (DSMC) method for the fundamental physical analysis of fluidic flows through narrow channels (14). Specifically, continuum theories can break down gas flows through narrow regions. Rarefaction effects, such as velocity slip and temperature jumps that have been microscopically and experimentally observed, were modeled using DSMC.

Fluid flows through microfilters were studied by DSMC. Microfilters designs are used to capture airborne particles such as bacteria, spores etc. The geometry of the simulated filters is shown in Figure 13. Three different sized filters were analyzed, and the dimensions of those filters are presented in Table I.

The simulations were started from a vacuum initial condition. The number of iterations was determined so that after the initial shock transversed the simulation domain, enough iterations had occurred to take noise free averages. All simulations were done on the NT-Supercluster and the Origin 2000 system.

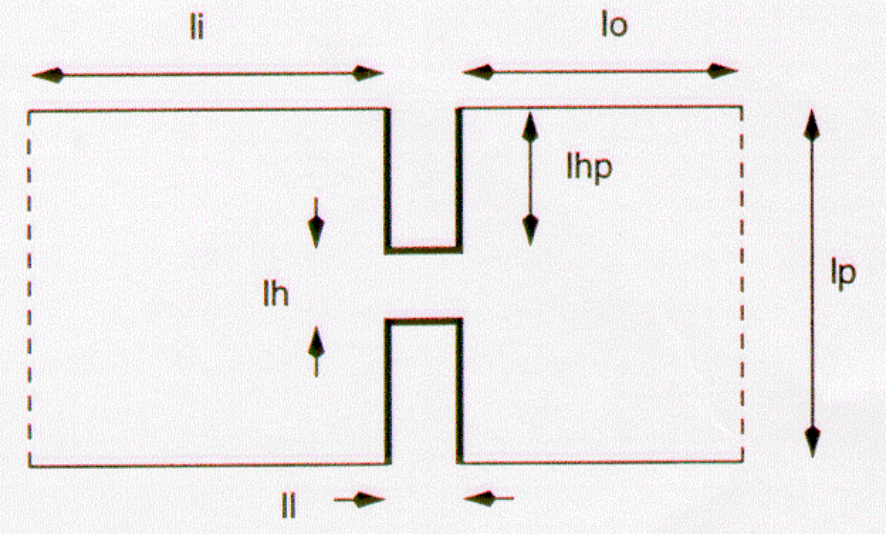

Figure 13. Geometry of the simulated filter element

Table I. Dimensions for Filter Elements (microns)

Element	li	lo	lp	lhp	lh	ll
1	5	3	5	2	1	1
2	5	3	5	2	1	5
3	1	1	1	1	0.2	1

The density, pressure, y-velocity component and the x-velocity component of the velocity for a microfilter of similar geometry are shown in Figures 14-17, respectively. Filter elements were simulated for a pressure difference of 0.15 Atm. In these figures the axes are in meters and the units of color axes are noted in the captions.

In Figures 18 and 19 are presented the changes in pressure and velocity along the flow direction though the centerline of the simulation domain. The individual curves are shifted along the x-axis to align the centers of the channels.

It was observed that for all cases the pressure drop was very close to linear. This was consistent with the linear increase in flow velocity along the channel observed for filter elements 2 and 3. For filter element 1, the velocity profile, together with the linear density drop, indicated a degree of nonlinearity. DSMC is an important technique to provide fundamental insight into the operation of the microfilters.

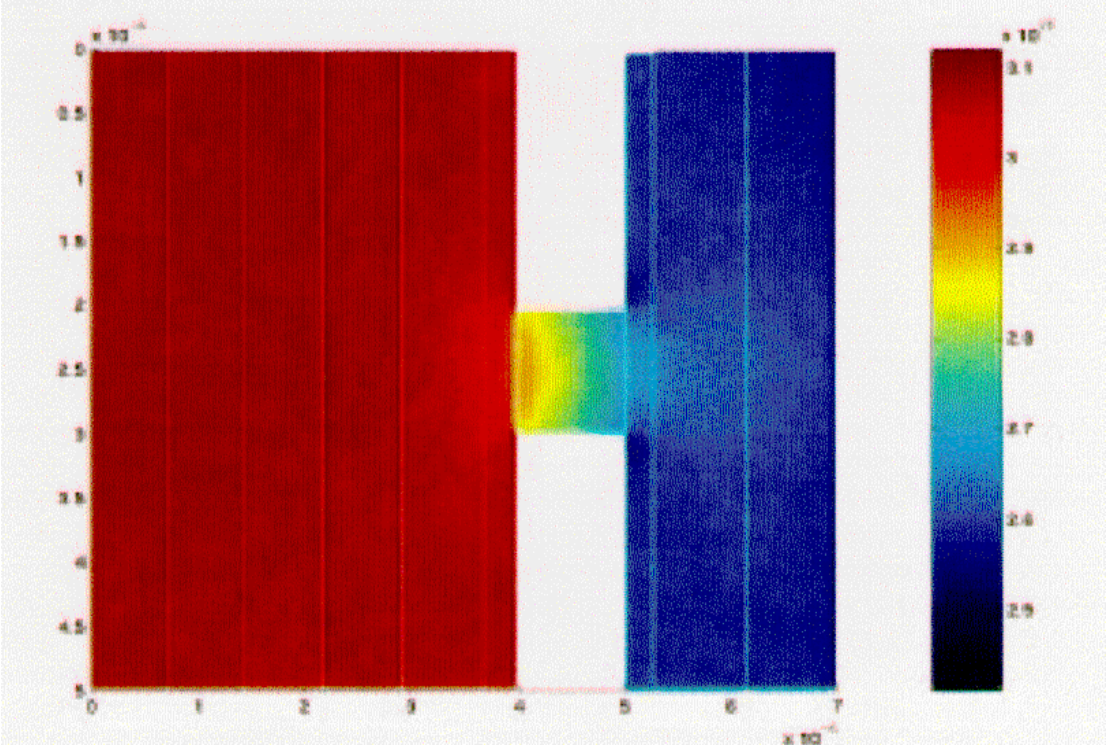

Figure 14. Density variations for a typical microfilter

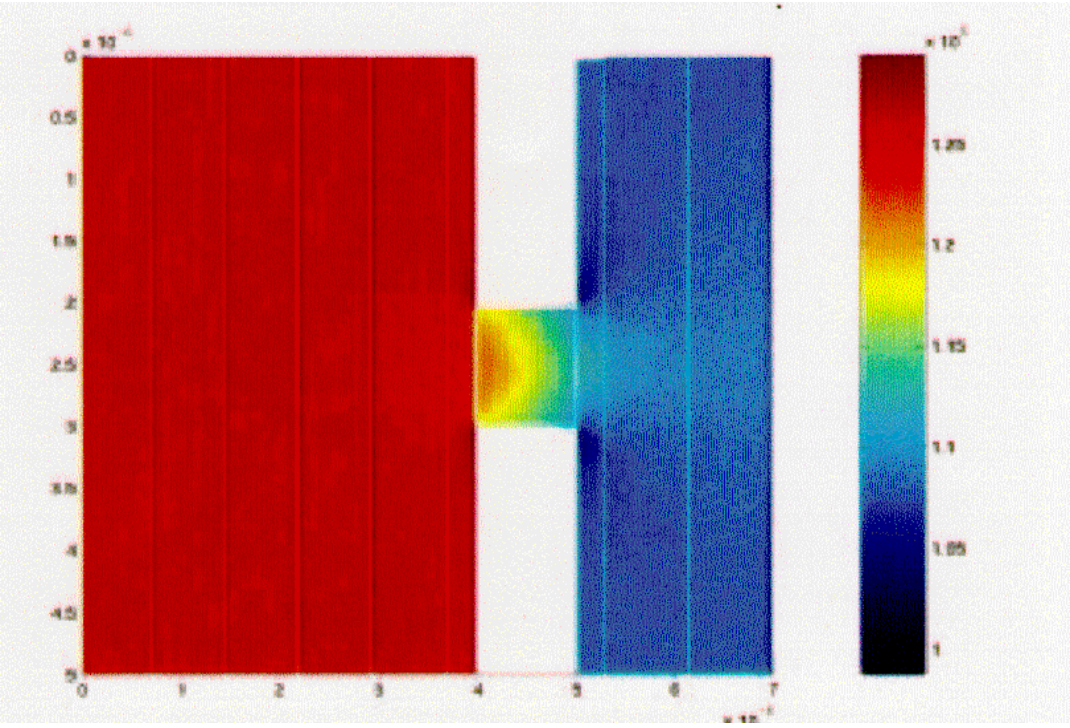

Figure 15. Pressure variations for a typical microfilter (kPa)

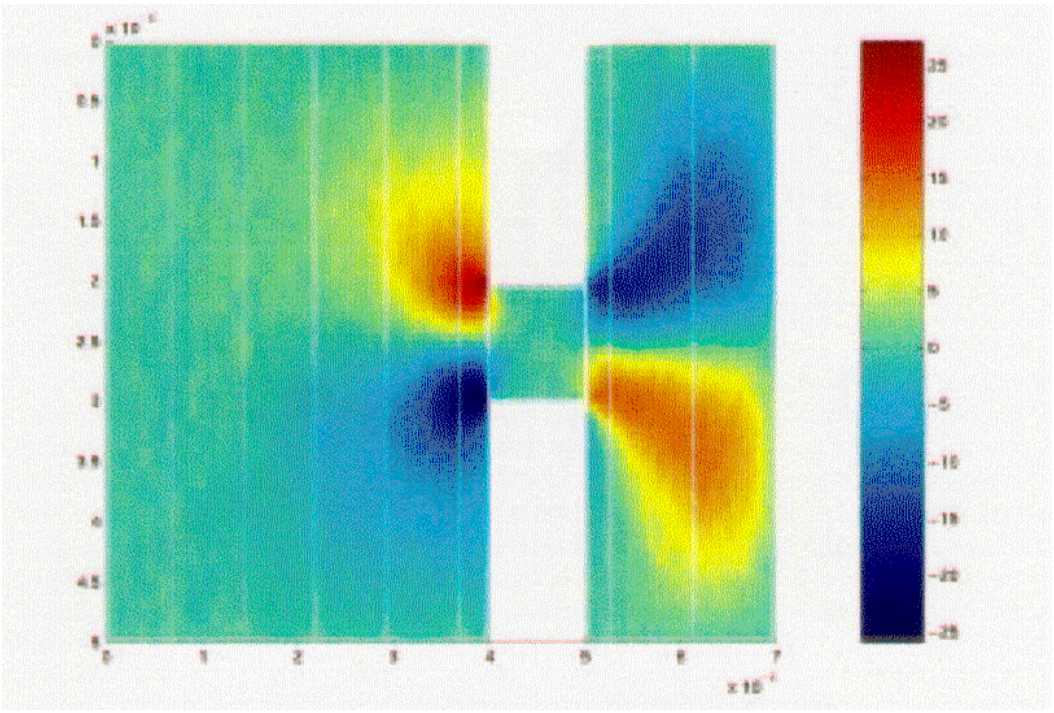

Figure 16. Y-velocity variations for a typical microfilter (m/s)

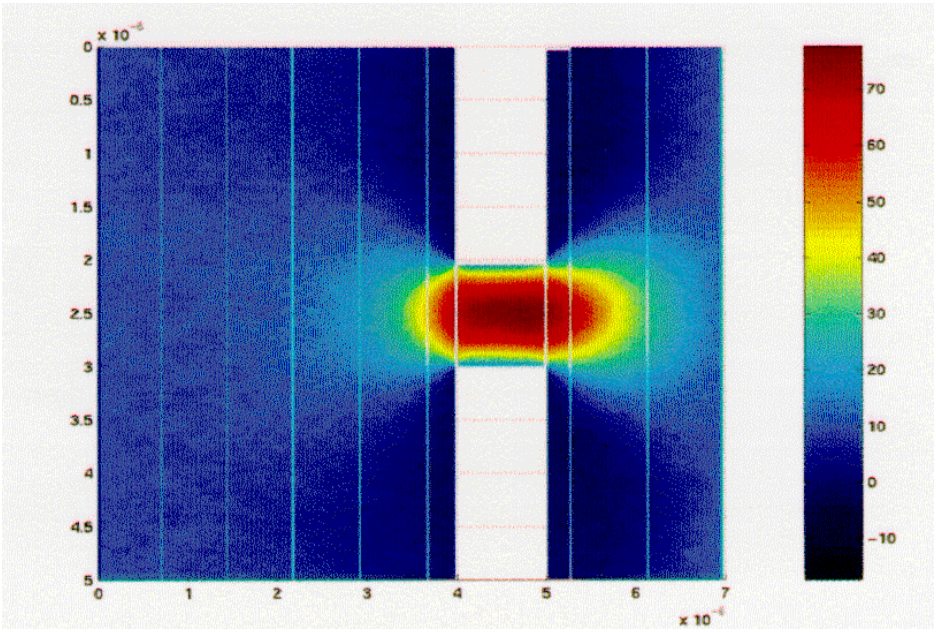

Figure 17. X-velocity variations for a typical micorfilter (m/s)

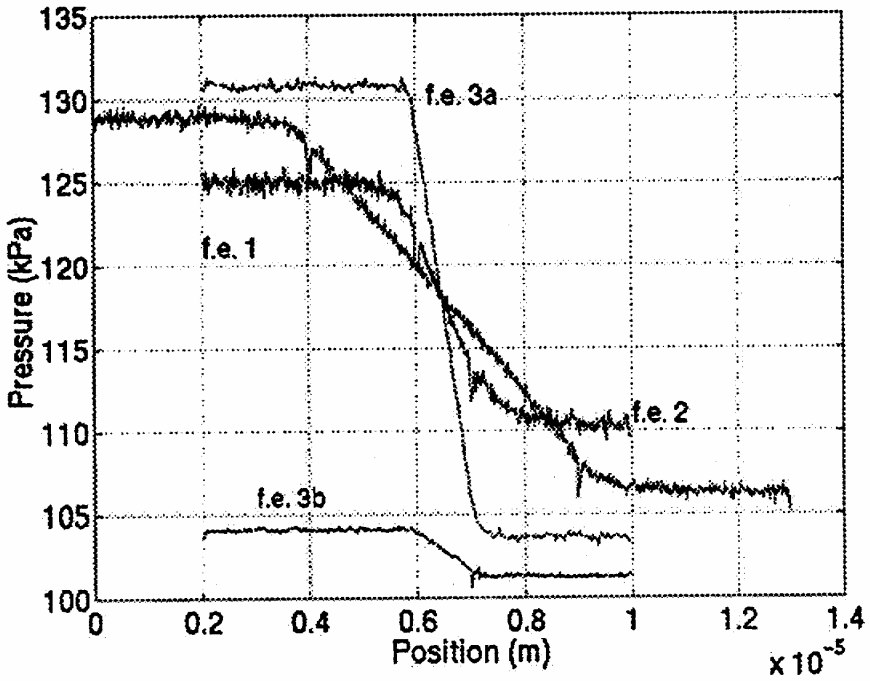

Figure 18. Variation of pressure along the mid-line

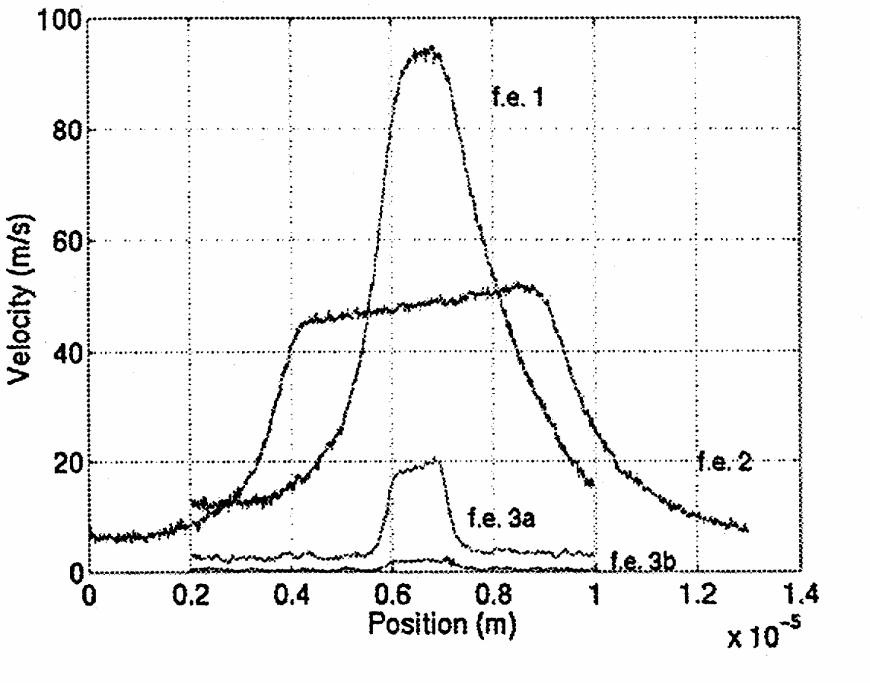

Figure 19. Variation of velocity along the mid-line

3.3.4 Multiscale Methods for Efficient Analysis of Microfluidic Devices

Multiscale methods for the efficient analysis of microfluidic devices have been developed, which are critical for the efficient and accurate analysis of microfluidic devices. A multiscale method is an approach where continuum Stokes and Navier-Stokes equations are combined with molecular approaches such as Direction Simulation Monte Carlo (DSMC) methods (15).

It was observed in the studies of microfilters that continuum theories broke down only in certain critical regions, and continuum theories were valid everywhere else. Complex microfilter designs were simulated with multiscale approaches. The design of dual-stage filter arrays for filtering particles of a certain size is practically impossible by using purely DSMC methods. By using multiscale methods, it was possible to perform fundamental studies. These multiscale methods were at least 100 times faster than the purely molecular approaches based on DSMC.

Modeling by coupling continuum and atomic scale algorithms for a simple Couette flow example is presented. In Couette flow (Figure 20) the fluid flows between two walls, one of which is fixed, while the second wall is moving. The exact solution in this case is linear, and differences due to incompatibility in the interface conditions cause the variation from linearity. The results of this DSMC analysis are presented in Figures 21-23. The green lines in these figures show the exact solution to the Couette flow, while the DSMC simulation solutions are the red dots. The solution at the interface matches with the DSMC solution, meaning that the interface conditions for the modeling are working properly and accurately.

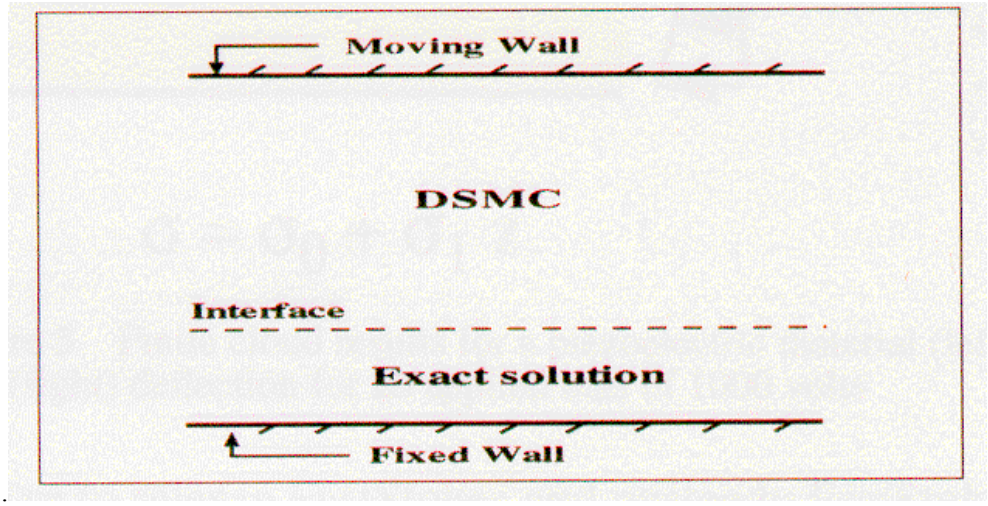

Figure 20. Diagram of Couette flow

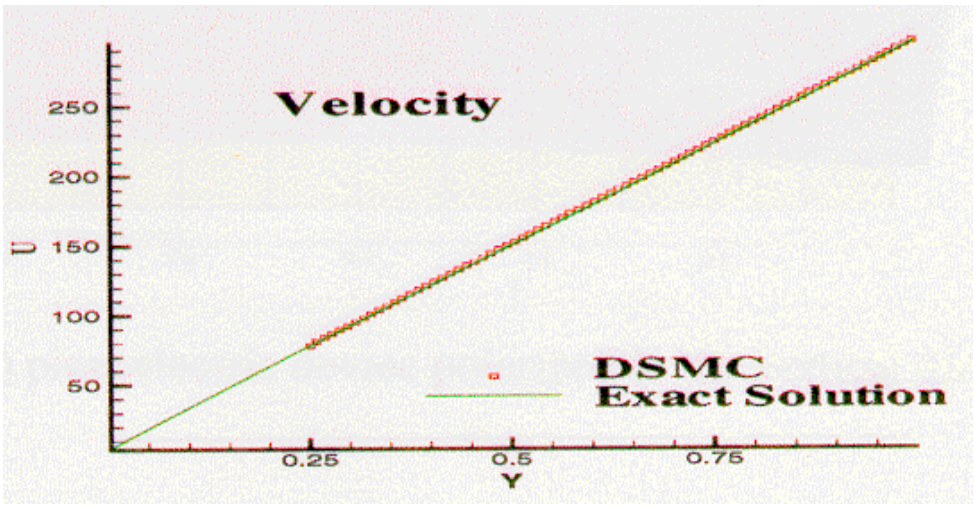

Figure 21. DSMC velocity results of Couette flow

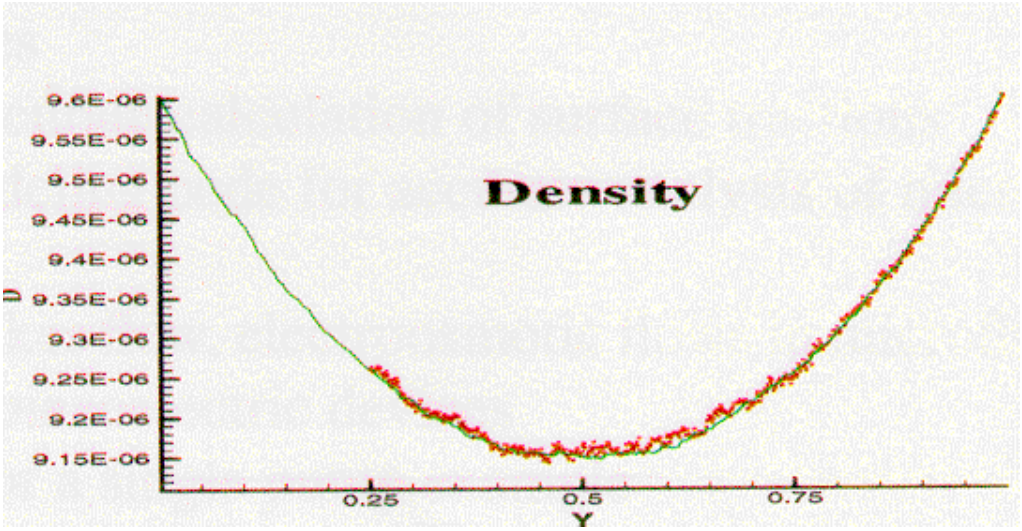

Figure 22. DSMC density results of Couette flow

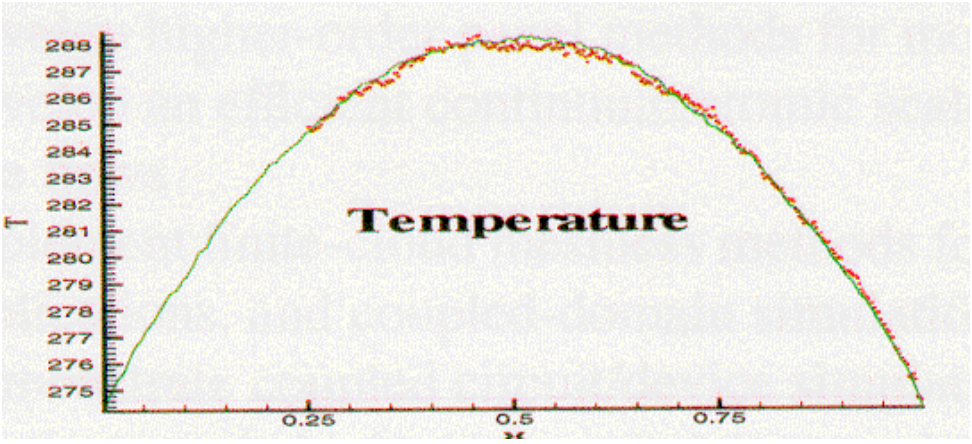

Figure 23. DSMC temperature results of Couette flow

4. COUPLED CIRCUIT/DEVICE MODELING

The overall goal of coupled circuit/device modeling was the development of a coupled circuit/microfluidic device simulator. Because of the tight coupling between the dynamics of the fluid flow and the control circuit, the response of the complete system can be accurately determined only from a solution of the circuit equations coupled to the microfluidics solver (numerical model). Such a simulation is unique in that it allows accurate simulation of a complete microfluidic system, *including the associated electronics*, whereby design tradeoffs can be readily evaluated. Summaries of coupled circuit/device modeling, and more details can be found in references 19-29.

4.1 PROTOTYPE COUPLED CIRCUIT AND MICROFLUIDIC SIMULATORS

Prototype coupled circuit and microfluidic simulators were developed based on the circuit simulator SPICE3 and the fluidic simulators Νεκταr and EOFLOW. The capabilities of this coupled simulator for a simple example illustrated by the block diagram in Figure 24. This system is made up of a micropump, a microflow sensor and an electronic control circuit. The electronic circuit adjusts the pump flow rate so that a constant flow rate is maintained in the channel. The flow sensor senses the flow rate that is controlled by the electronic circuit controlling the pump.

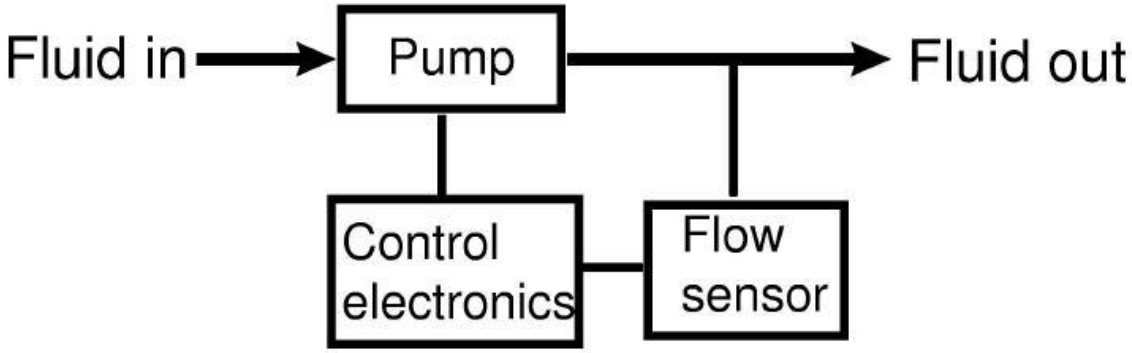

Figure 24. Block diagram of a microfluidic system

For the purposes of this example it is assumed that the micropump has a piezoelectric actuation for its membrane and the microflow sensor is an anemometer type of flow sensor. There are four different physical domains (electrical, structure, fluid, and thermal) that must be considered for a complete system level simulation. These domains are coupled to one another as follows:

- Electromechanical coupling for piezoelectric actuation of the pump membrane
- Fluid-structure coupling due to volume displacement of the pump membrane
- Fluid-thermal coupling because of the thermoresistor cooling the fluid for an anemometer type of microflow sensor
- Electrothermal coupling for thermoresistor heating due to current flow in the microflow sensor

The overall system is simulated using a combination of coupled solvers, compact models and lumped elements. Simple elements are implemented as lumped elements or compact models. These elements are the electromechanical transducer (piezoelectric actuator) and thermoresistors.

4.2 PROTOTYPE FLOW SENSORS

Flow sensors are much more complicated but often the fluid flow in sensors is relatively simple. For example, if the fluid flow has a constant parabolic profile for the velocity, then it is possible to use compact models for the flow sensors as well. It is important to note that these compact models are parameterized and can be highly nonlinear. These models are obtained by insight gained from detailed physical level simulations. Usually pumps operate in a nonlinear mode of fluid flow with a strong fluid-structure interaction. Therefore, a detailed physical level simulation of the pump is required.

In this example, the electromechanical actuator, thermoresistors and flow sensors are described as lumped elements and/or compact models. The pump is modeled at the detailed physical level. All lumped elements and models are implemented in SPICE3. The pump is implemented as a direct SPICE3-Νεκταr interconnection (Figure 25). SPICE3 transfers the time t_{spice} and pressure P for membrane actuation and to receive the flowrate Q and the time t_{call} for the next call from Νεκταr.

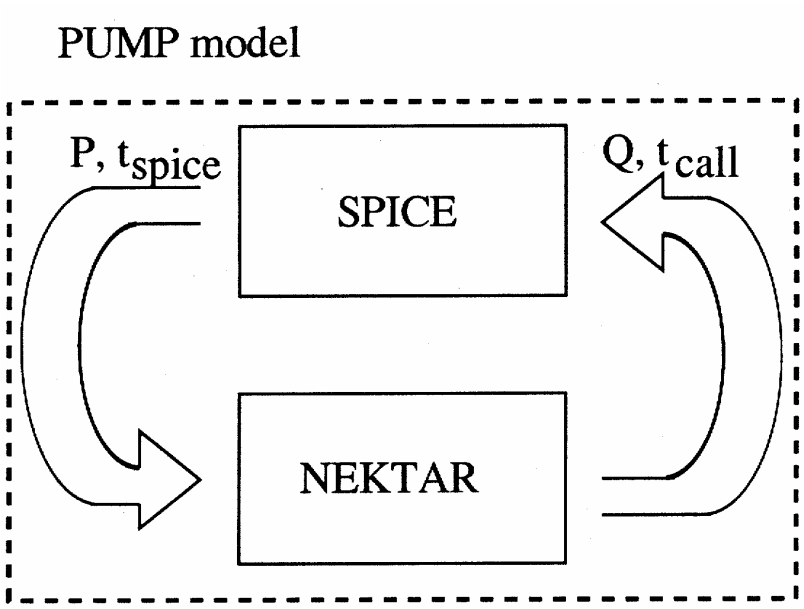

Figure 25. The SPICE3- interaction for the pump microsystem

The model for electromechanical coupling with a piezoelectric actuation of the membrane is shown in Figure 26. This model forms the interface between the electrical and mechanical networks. The electrical characteristics of the piezoelectric actuator are described by the capacitor C. The input voltage v translates into an output pressure P by virtue of the piezoelectric effect with coefficient k to activate the pump membrane. The mechanical characteristics of the piezoelectric actuator are coupled with the mechanical characteristics of the substrate.

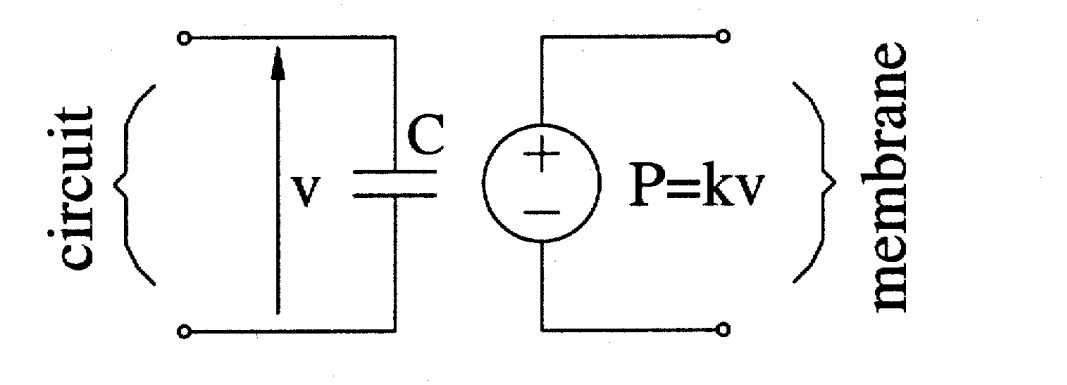

Figure 26. The lumped model for piezoelectric actuation

4.3 ANEMOMETER FLOW SENSOR

An anemometer type microflow sensor Macromodel has been developed using neural networks. The numerical solutions of Partial Differential Equations (PDE's) describing the microflow sensor were used as training data for the neural networks. This model is simple and accurate and has been verified with numerical simulations for a wide range of sensor parameters. The model incorporates both the steady state and the dynamic responses of the flow sensors. The model has been implemented in SPICE3 and can be used for simulating the flow.

In Figure 27 are presented PDE temperature solutions for a microflow sensor with zero fluid flow in the channel (a), and with flow (b). The height of the channel was 20 microns. In Figure 28 are presented the PDE's modeling results of the change in temperature verses distance for a 50-micron channel height. Superimposed on this figure is experimentally measured temperature differences, which validates the PDE model.

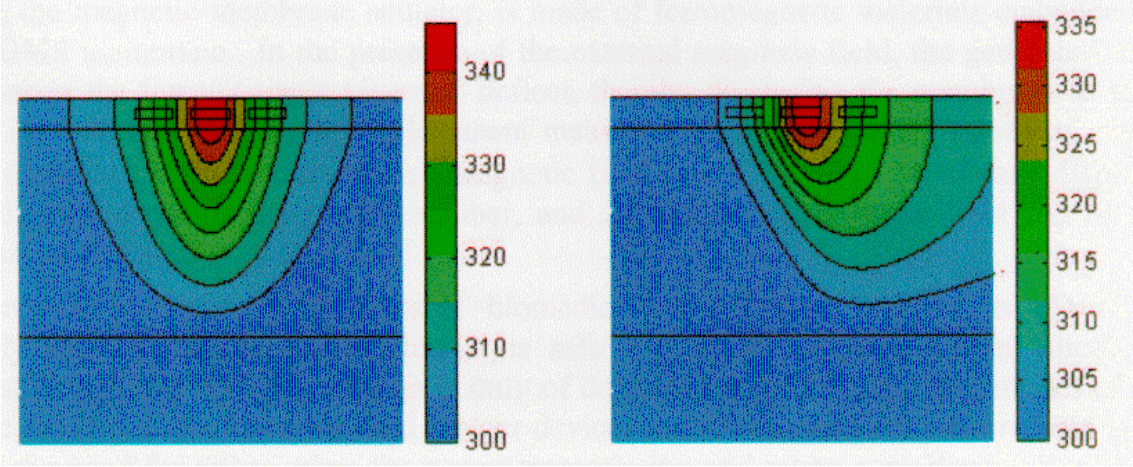

Figure 27. PDE resultant temperatures (Kelvin) for a microflow sensor with zero flow (left) and with flow (right)

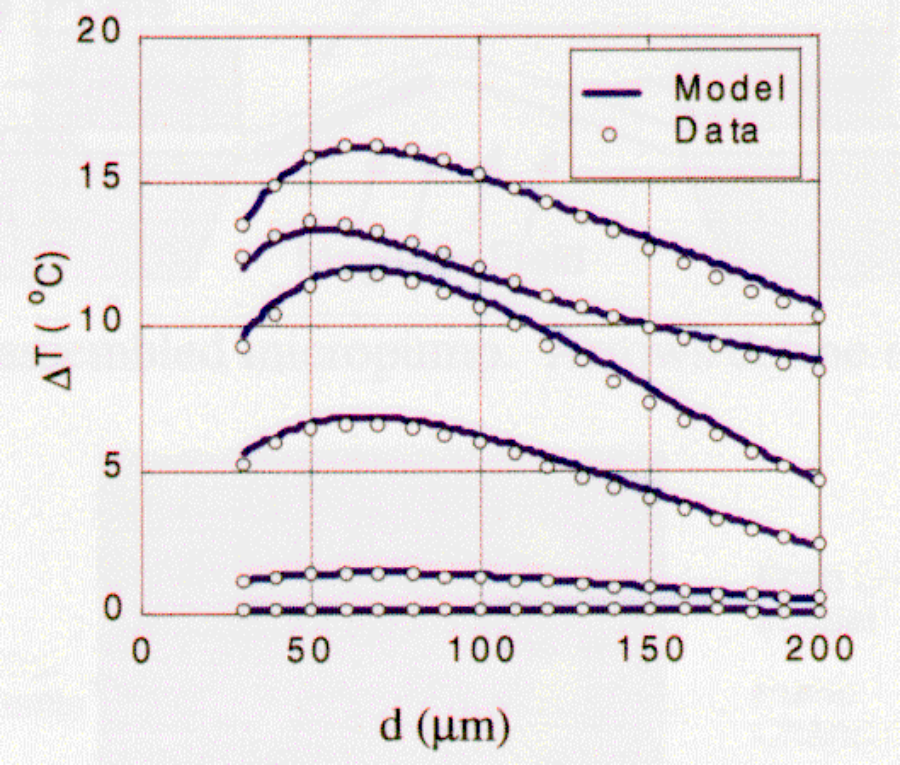

Figure 28. The prediction accuracy of the neural network based model for a channel height of 50 μm

4.4 COMPLETE SYSTEM FOR SIMULATION

The structure of a complete anemometer type flow sensor is shown in Figure.29, a macromodel has been developed (16,17). This macromodel is based on neural networks trained using data (Figure 30) from detailed physical simulations.

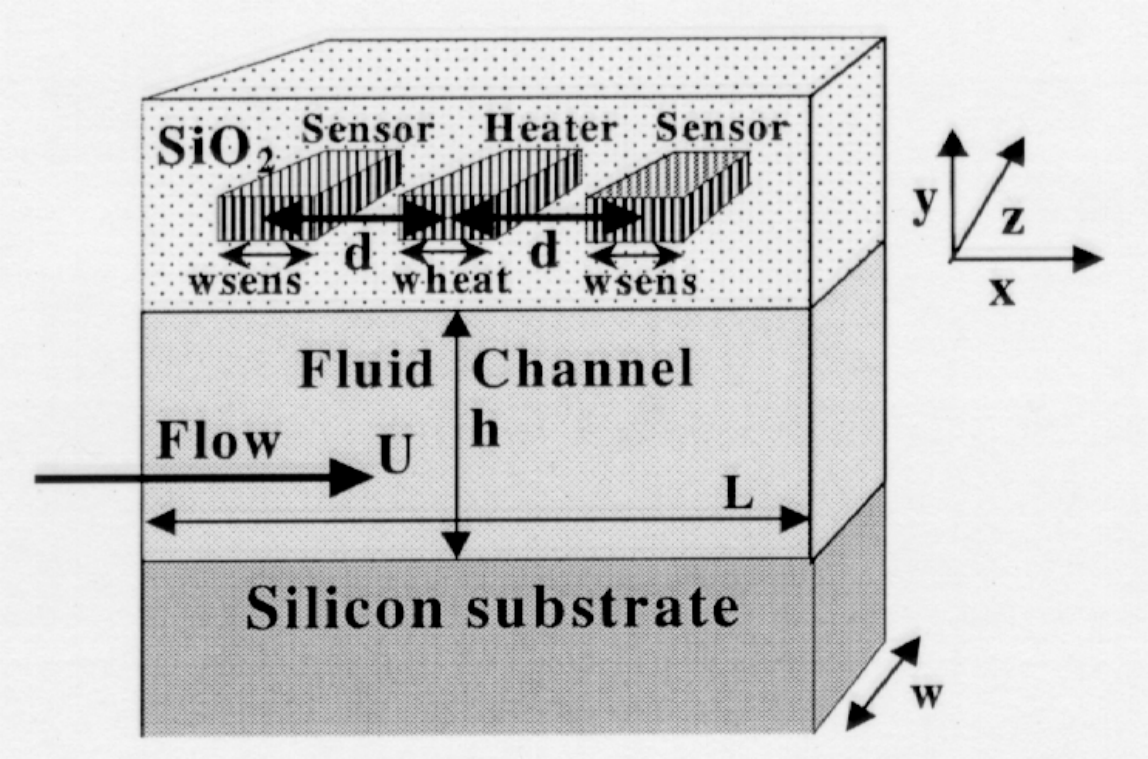

Figure 29. The structure of an anemometer type microflow sensor

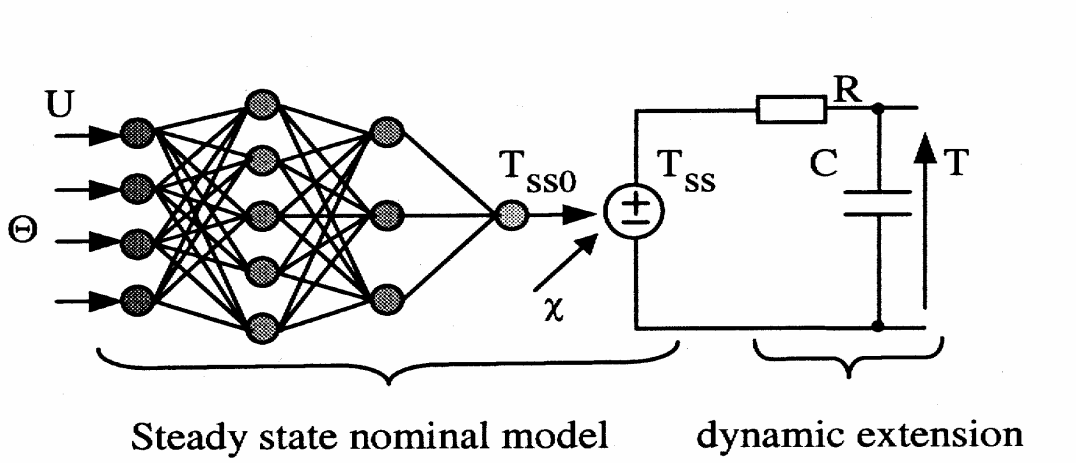

Figure 30. The dynamic macromodel for the flow sensor

The steady-state solution T_{SS0} corresponds to a nominal power for the heat source χ. The neural network output T_{SS0} is a multivariate function of the flow velocity U and the vector of geometrical and physical parameters Θ. T_{SS} is a linear function of the heat source χ and T_{SS0}.

The inputs to the neural network are the flow velocity U and the vector of geometrical and physical parameters Θ. The results from this model are in good agreement with the simulated data for a large range of parameters. The dynamic macromodel is incorporated in SPICE3 by coupling with a sensor circuit and a model for thermoresistors for the heater and sensors.

A simplified schematic of the complete system for simulation is shown in Figure 31. In this system, the flow rate Q determines the flow sensor velocity U for a given set of geometry parameters (h, d, wsens). Based on the fluid flow rate the thermoresistor temperatures, T1, T2 and T3, change which in turn alters the resistance values R1(T1), R2(T2) and R3(T3). The resistance R1(T1) and R3(T3) are included in a Wheatstone-bridge arrangement with two fixed resistors R4 and R5. The voltage difference, V_{R3}-V_{R1}, is directly proportional to the temperature difference T3-T1. This voltage difference is linearly transformed to the output voltage Vout by an operational amplifier with a controlled gain. This output voltage determines the pressure P, which activates the pump membrane and changes the flow rate Q. The thermoresistor of the heater (R2) is activated by the control electronics that maintains a constant heater temperature.

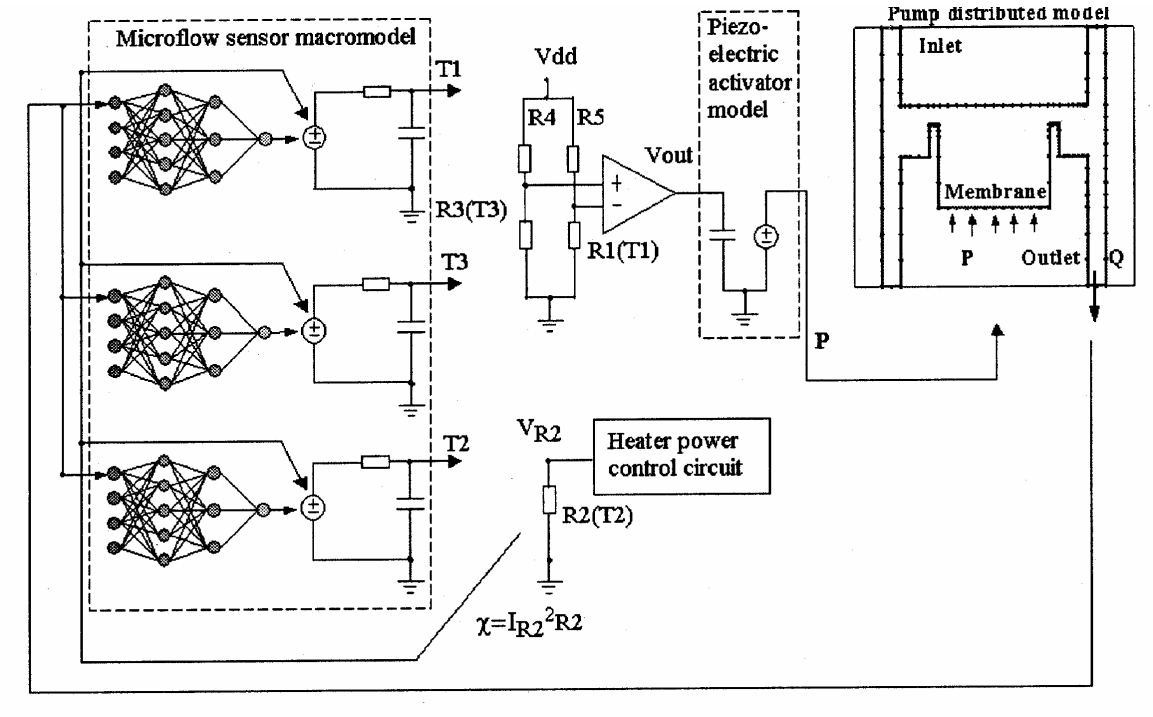

Figure 31. A description of the complete system for simulation

The circuit simulator SPICE3 is chosen as the controlling solver since it has automatic time step control, and supports lumped-element equivalent circuits. Furthermore, models for different abstraction levels can be easily implemented in SPICE3. is embedded as a subroutine in SPICE3. The interaction with SPICE3 is by means of the model code and the simulation engine. Synchronization timepoints are determined and used by the SPICE3 transient analysis engine. The pump is modeled as a SPICE3 element with being the underlying simulation engine. Lumped element descriptions and/or compact models describe the other elements in the circuit.

The simulation results from the coupled simulator are presented in Figure 32. In this simulation, one can determine the pressure on the pump membrane, the flow velocity, and the output control voltage as a function of time for various component parameters. In this simulation, the structure of the pump and the structure's influence on overall system performance can be easily determined. The coupled simulator provides valuable information to the system or device developer.

The flow pump rate Q determines the flow sensor velocity U. This yields the temperatures for the sensor thermoresistors. The difference between the resistance values R1(T1) and R3(T3) is transformed into the voltage Vout by the control electronics. Vout is used to control the pressure P for the pump membrane that in turn determines the flow rate Q.

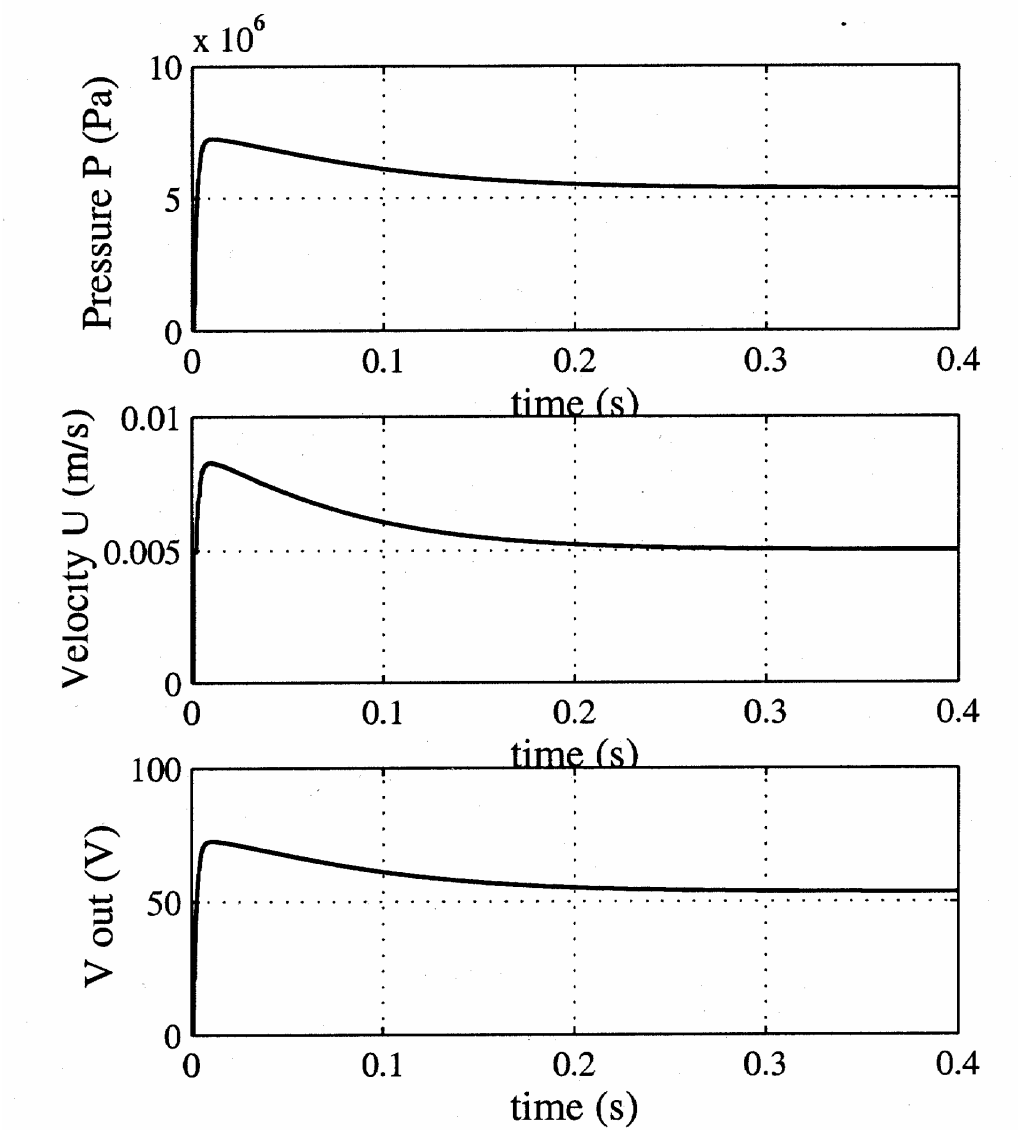

Figure 32. The pressure, velocity and output voltage for the simulation example as a function of time

SPICE3 and EOFLOW simulator codes were modified to enable coupled simulation with any number of interconnected cross channels (Figure 33). The results for SPICE3/EOFLOW coupling are briefly described. A system described by a mesh of 10x10 interconnected cross channel pipes was simulated to demonstrate the advantages of the coupled simulation environment. Voltage sources with different amplitude and frequency were connected to every outlet as shown in Fig. y. The response was checked near the center of the mesh. A transient analysis for 300 μs took an hour of simulation time on a Sun Solaris with UltraSparc 440 MHz processor. The goal of this simulation was to check the voltage calculation at the interconnection point of the two channels.

The resulting output signal contains all harmonics corresponding to input frequencies with amplitudes as expected. The goal of this simulation was to check the voltage calculation at the interconnection point of the two channels. The resulting output signal contains all harmonics corresponding to input frequencies with amplitudes as expected. Figure 34 shows one period of output waveform and Figure 35 contains the spectrum of output waveform.

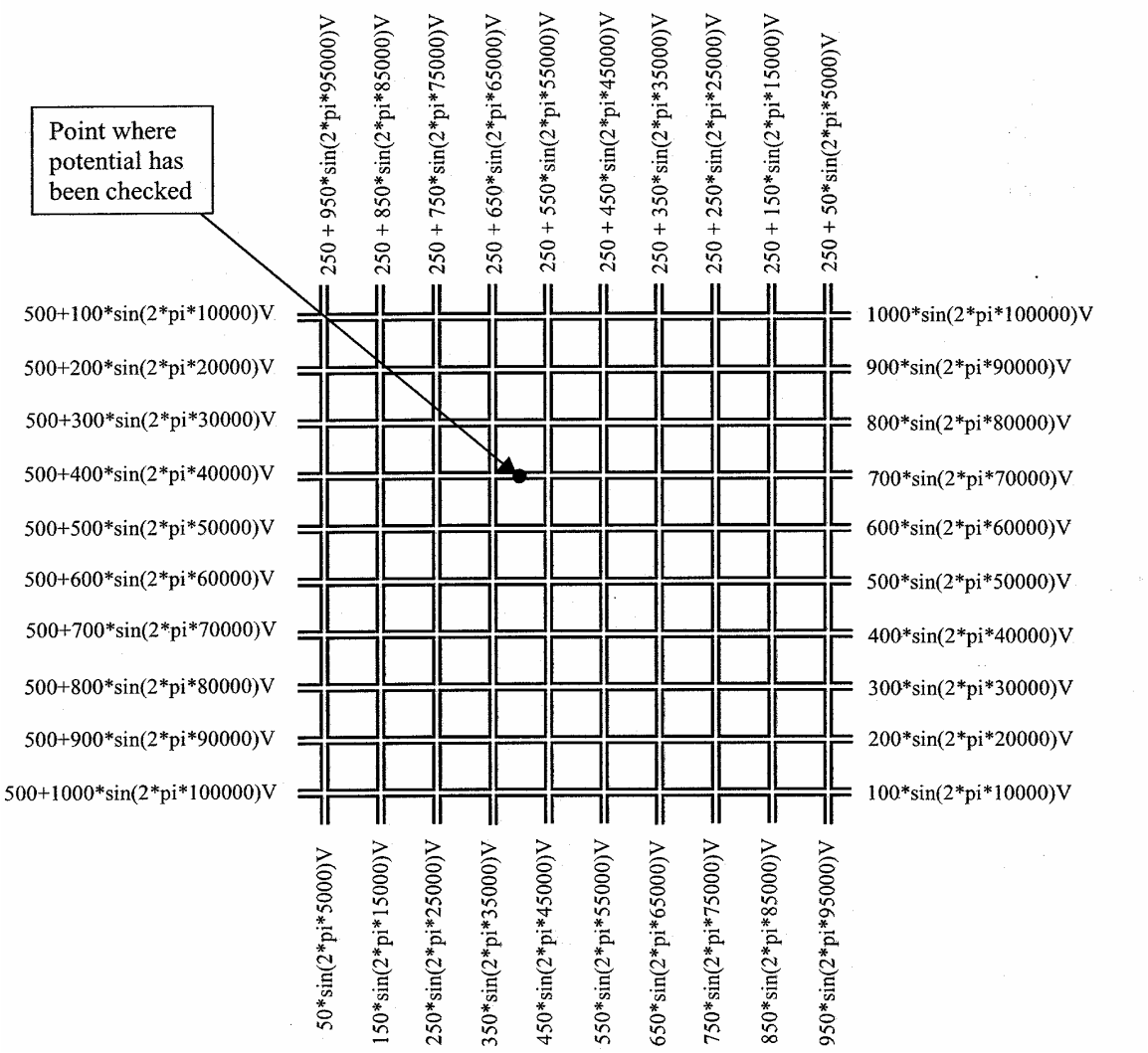

Figure 33. 10x10 cross channel mesh simulated with applied voltages at all outlets

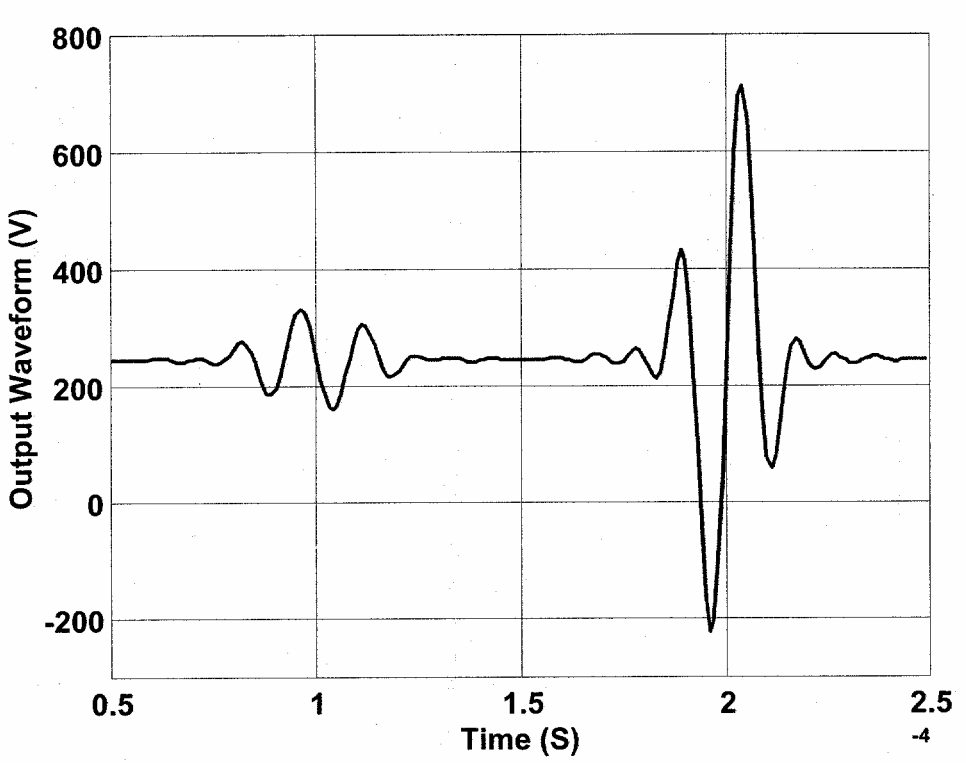

Figure 34. One period of the output signal

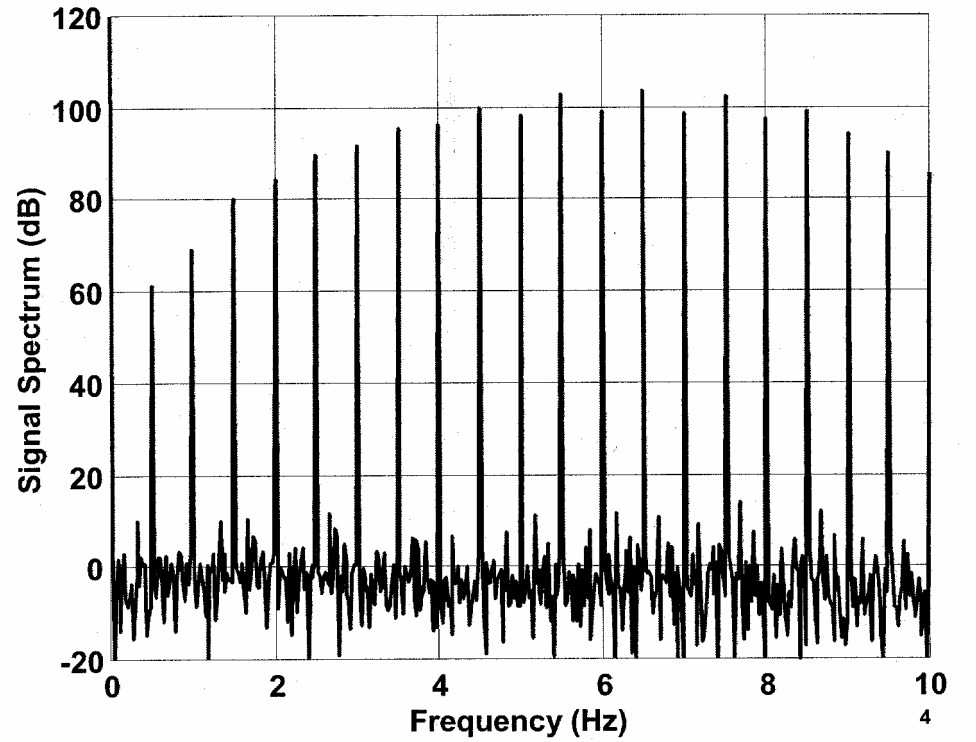

Figure 35. Spectrum of the output signal

SPICE3/EOFLOW simulator codes were modified to implement a new crosschannel model in SPICE. Other code modifications were made to enable coupled simulation with two interconnected crosschannels. A microfluidic system containing two cross channel pipes (Figure 36) was simulated. The goal was to check the voltage calculation at the interconnection point of the two channels. These results match the previous results obtained for the simulation of one cross channel pipe.

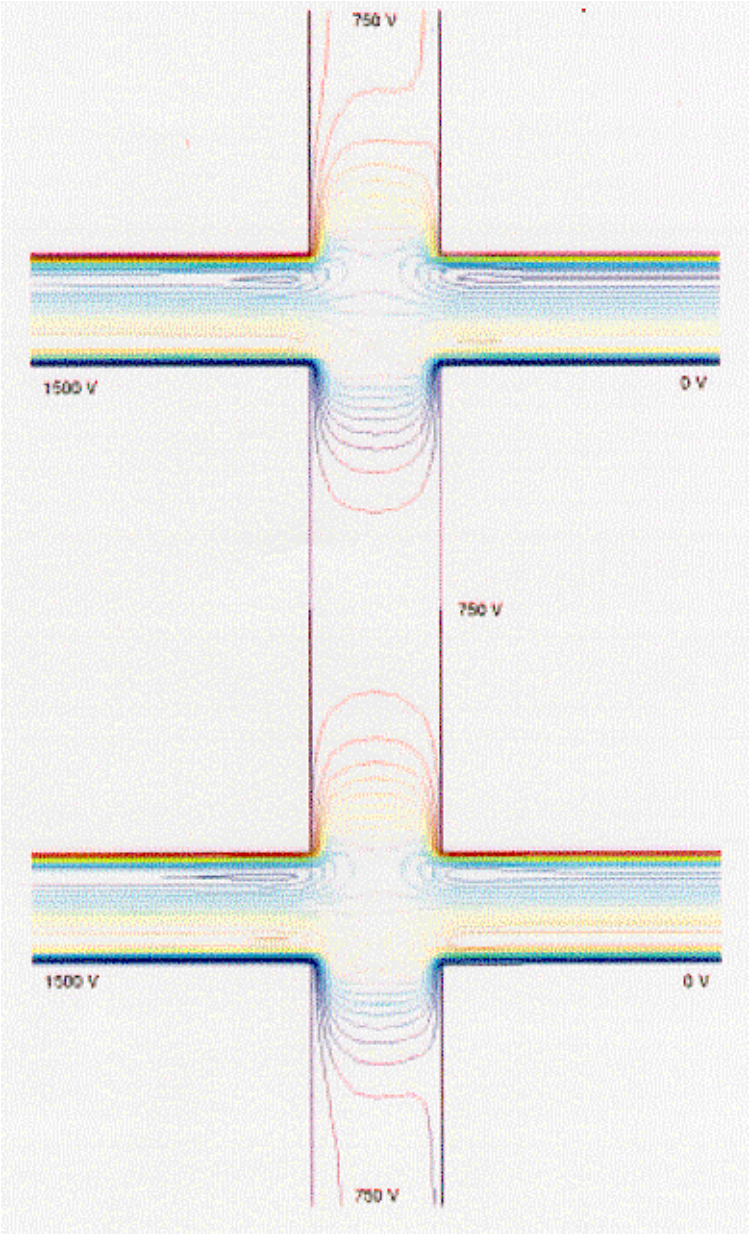

Figure 36. Example of two cross channel pipes simulated during one of the time steps in the transient analysis

4.5 ELECTROOSMOTIC FLOW SIMULATOR

The code for the electroosmotic flow simulator was modified to correct memory leakage problems. Other code modifications were made to provide reliable and efficient circuit/microfluidic device coupling. The electroosmotic flow simulator was adapted for repeated calls with restart capabilities. The circuit/microdevice is based on a generic microfluidic device model that allows use of different solvers in a similar manner.

Applications to microfluidic system design based on the electroosmotic effect were demonstrated. A microfluidic system consisting of a cross channel pipe driven by control electronics (Figure 37) was simulated. The control electronics implements an integral type controller and produced an output that is an integral of the flow rate through the vertical channels. The goal of this system was to obtain zero flow rate through the vertical channels by automatically determining the voltages applied to the vertical channels. Simulation results (Figure 38 and 39) show the dynamic behavior of the whole system. This simulation provides the basis for future simulation of separations and dosing systems for biomedical and chemical application such as a micro total analysis system.

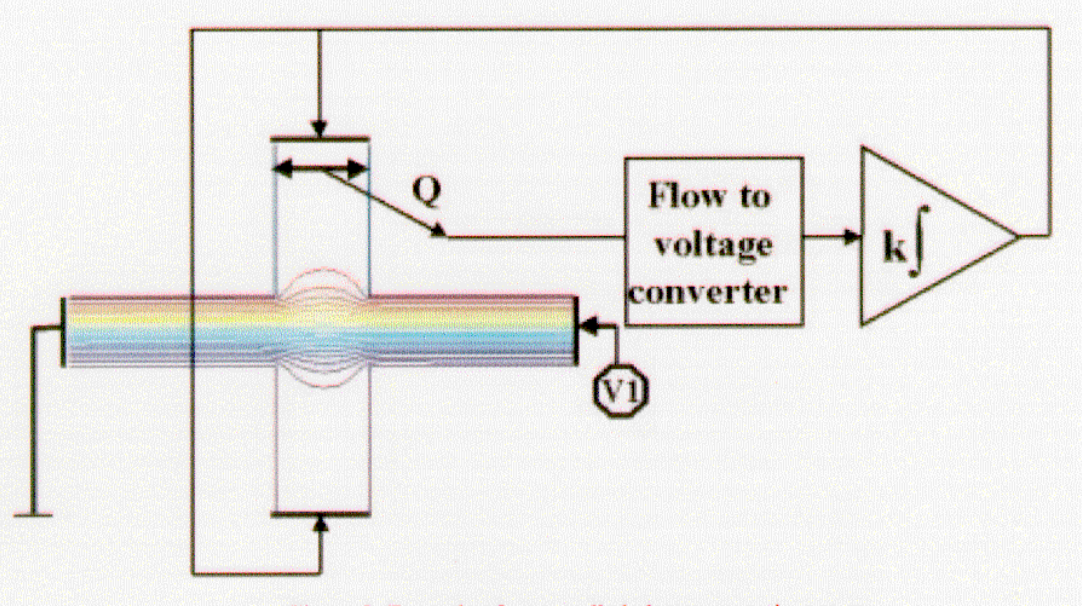

Figure 37. Example of a controlled electroosmotic system

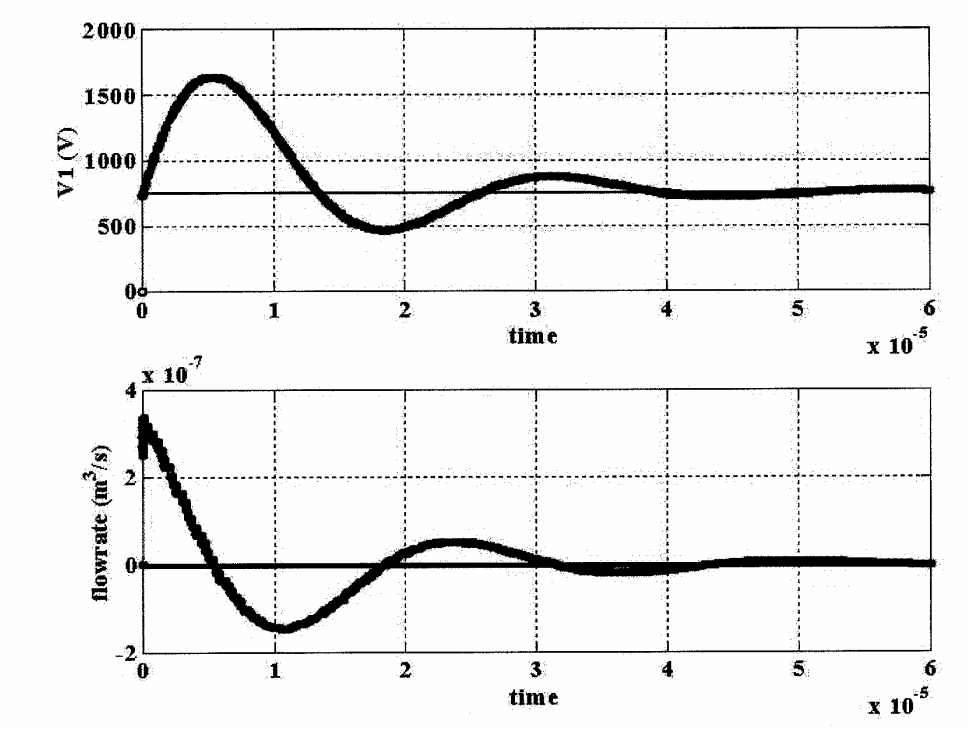

Figure 38. Dynamic behavior of the control potential and the flow rate for the electroosmotic system

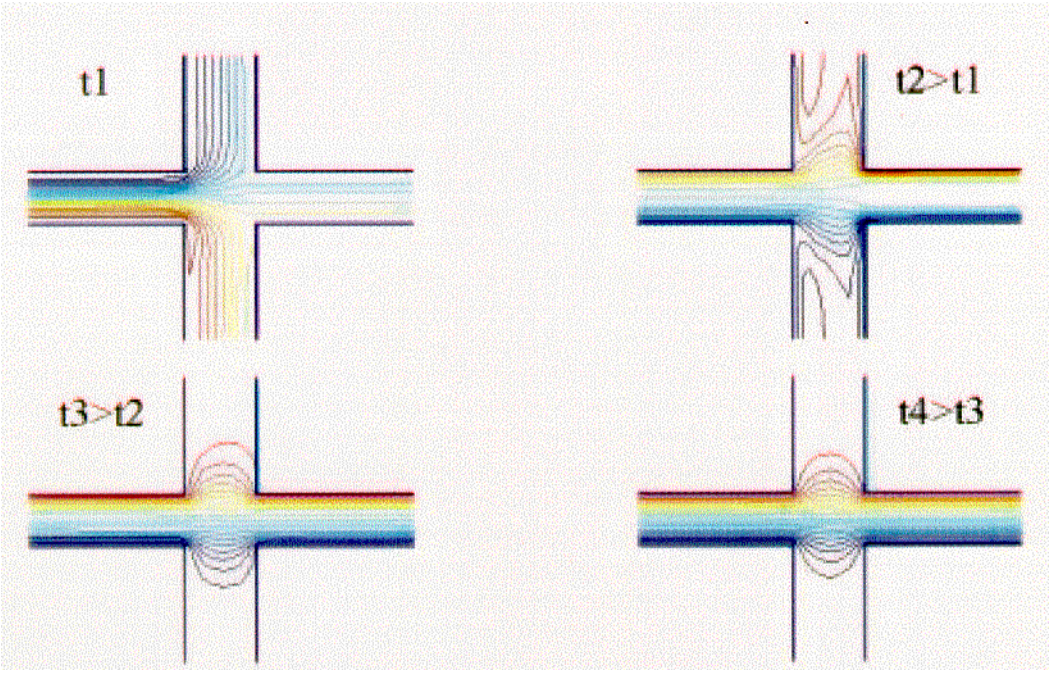

Figure 39. Dynamic behavior of streamlines for the electroosmotic system

5. EXPERIMENTAL EFFORT

Summaries of the experimental work are presented here, and more details can be found in references 30-33.

5.1 FABRICATION

New materials have been used for the first time in MEMS fabrications, and novel devices have been fabricated for the first time.

5.1.1 Materials

Liquid crystals and biodegradable polymers have been used as microfluidic materials.

5.1.1.1 Liquid Crystal Polymer as a Microfluidics Material

Recently, new techniques using low-cost organic polymers have been studied. Fluid circuits realized using photoresist, parylene, and PDMS (18) have been demonstrated. However, a common difficulty encountered in preparing PDMS microfluidic devices is the relative weak bonding between PDMS and other materials - lateral leakage is a major concern for such fluid devices.

The liquid crystal polymer (LCP) is a thermoplastic polymer material with unique structural and physical properties. It contains rigid and flexible monomers that link to each other. When flowing in liquid crystal state, the rigid segments of the molecules align next to one another in the direction of shear flow. Once this orientation is formed, their direction and structure persist, even when LCP is cooled below the melting temperature. This is different from most thermoplastic polymers (for example Kapton), whose molecules are randomly oriented in the solid-state.

An alternative process for fabrication a fluid channel using LCP/glass assembly was developed (19). Compared with other methods of forming glass fluid channels, LCP has several unique advantages. First, LCP films are virtually impermeable by liquid and gas. Such a property may be important in situations where liquid and gas diffusion is undesired. Secondly, whereas PDMS can be bond to glass by natural adhesion force, LCP can be attached to glass with much stronger bonding developed through the lamination process. Such bonding strength is important for retaining the integrity of the fluid chip. Commercial LCP films are also with a lower cost compared to PDMS. Thirdly, LCP to glass bonding requires much lower temperature and shorter processing time compared with glass-glass bonding.

5.1.1.2 Pyrex Glass Wafers as a Microfluidics Material

Microchannels on a pyrex glass wafer were fabricated for the first time (20). This glass wafer was patterned by using photolithography process with gold mask and etched in HF to form a 70-μm deep trench. A LCP film was then thermally laminated on the

glass wafer with the glass heated to 260^{o}C on a hotplate. The lamination of LCP is conducted by applying moderate pressure using a roller. Via holes through LCP film to glass channel reservoirs were produced using mechanical punching or laser drilling. Plastic inlet and outlet pipes were bonded on LCP film with epoxy as the reservoirs.

The functionality of such micro fluid channels in electrophoresis tests was demonstrated (21). The LCP-glass assembly was first immersed in TBE buffer solution and degassed 20 minutes in a vacuum chamber to fill the entire channel and remove trapped air bubbles (22). Fluorescent beads were then injected into the fluid channel through one of the inlets. Platinum electrodes were inserted at the inlet and outlet reservoirs. The hydraulic potential was completely balanced before electrophoresis was processed. When 50 V/cm was applied across the channel, the speeds of flowing fluorescent beads varied from 36~60 μm/s at different locations in the channel system.

As an alternative microchannels in LCP film were created. An Aluminum layer was first deposited on LCP film. This Al layer was patterned by photolithography to form a mask of micro channel. The LCP film was then etched to desired shape and depth by RIE using the Al mask. After etch completion, the Al mask was stripped away to release LCP film. This LCP film with the fluid channel on it was thermally bonded to a glass substrate. An SEM micrograph (Figure 40) clearly demonstrates the cross-section view of the channel. This potentially allows LCP channels to be bonded to other flexible films, such as another LCP film.

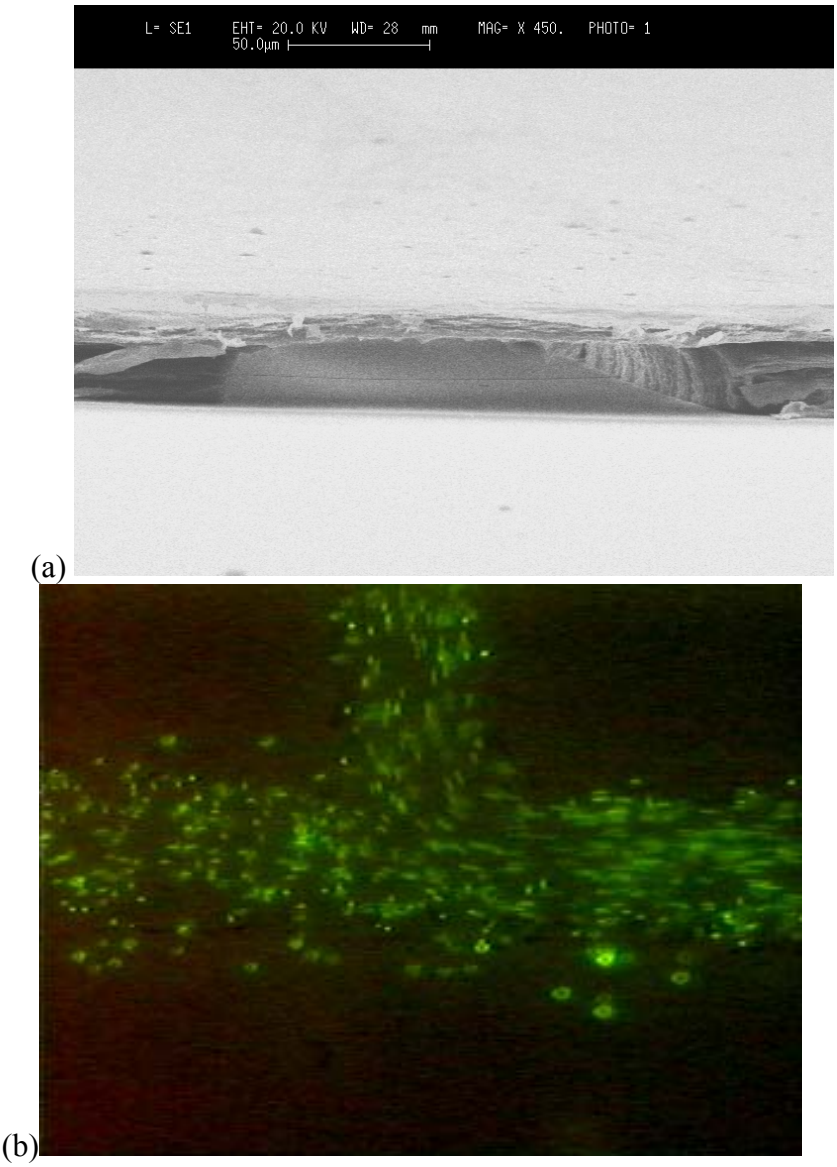

Figure 40. (a) SEM micrograph of a sealed LCP microchannel; (b) images of fluorescence beads moving inside a micro channel

5.1.1.3 Biodegradable Polymer as a Microfluidics Material

We report the development of micromachining techniques for a biodegradable polymer for the first time (23,24). By virtue of their ability to naturally degrade in tissues, biodegradable polymers hold immense promise as new materials for implantable biomedical microdevices. This work focuses on establishment of microfabrication processes for biodegradable microstructures and microdevices. Three unique fabrication processes have been established: (1) micro-molding process to form 3D microstructures in polycaprolactone (PCL) via a silicon micromachined mold; (2) a method of transferring metal patterns to surfaces of PCL substrates; (3) techniques for sealing both dry and liquid-filled PCL micro-cavities with a metal thin film (e.g. gold). Chemical

compatibility of PCL with common micromachining chemicals has been investigated (Figure 41).

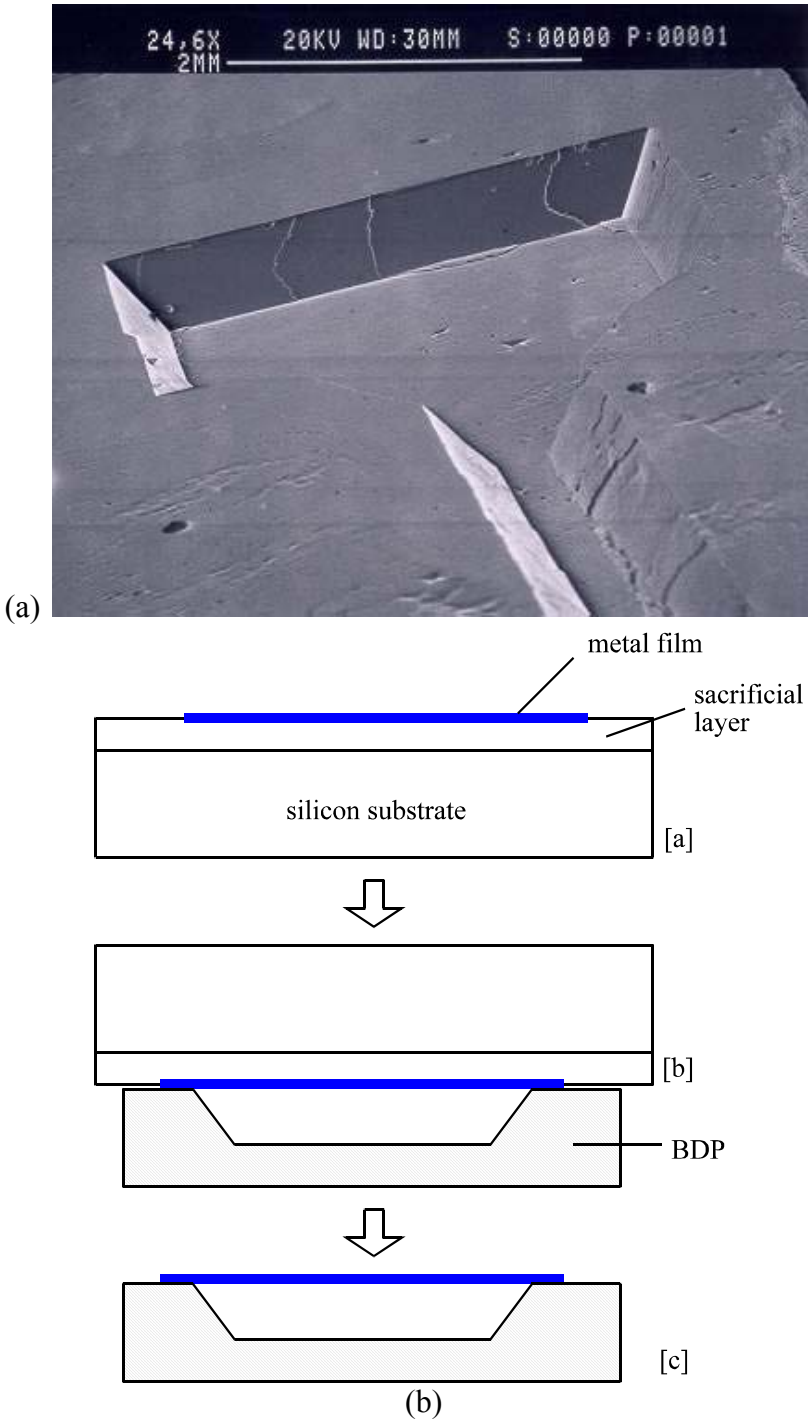

Figure 41. (a) SEM micrograph of a micromachined channel in BDP; (b) fabrication process for a sealed cavity in BDP

5.1.2 Microfluidic Components

Microfluidic components including channels, pumps and valves were fabricated. Flow visualization methods were developed to characterize these components. Also, a micro fabricated, externally powered magnetic diaphragm pump for telemetric operation of microfluidic systems was fabricated, as was a micro magnetic mixer for rapid, on-demand mixing of fluidics.

5.1.2.1 Magnetic Micro Pump

A tetherless micro magnetic membrane pump was fabricated capable of remote operation using an external magnetic field (due to the long-range forces provided) (25-28). The basic structure of the fully assembled pump is illustrated in Figure 42, which shows Layer I placed on top of Layer II. A fluid flow rate of 1.2-μl/min was measured at a pumping frequency of 2.9-Hz in the presence of a 2.85×10^5-A/m oscillating external magnetic field.

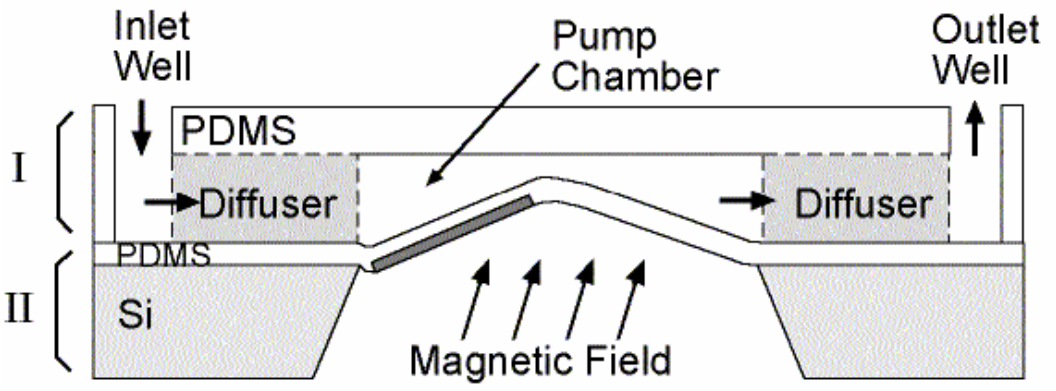

Figure 42. Schematic diagram of a magnetic actuated micro pump

Layer I, which consisted of the diffuser elements (which control one-way fluid flow), pump chamber, micro channels, and inlet/outlet wells, was fabricated using polymer micromachining techniques. The material used is a flexible, transparent silicone elastomer, polydimethyl siloxane (PDMS). Due to strong PDMS-PDMS bonding, Layer I can thus be self-bonded to Layer II (which has a thin PDMS membrane) by pressing the 2 layers together.

Layer II, the magnetic membrane actuator, is made of ferromagnetic materials embedded within a thin PDMS membrane. In the presence of the external magnetic field, the generated magnetic torque causes the ferromagnetic pieces to deflect, thereby displacing the membrane as shown in Figure 42. Maximum membrane displacement measured (using our present strongest magnet) is 83.9 μm under a 2.85×10^5-A/m external magnetic field. Membrane displacement thus pushes fluid out of the pump chamber, and an oscillating magnetic field can be used to affect pumping action.

This pump is suitable for implantable biomedical microfluidic systems as (1) PDMS is physically and chemically stable, thus it is safe and more compatible than silicon for an implanted device, (2) material damage is only of concern for ~ 5x higher magnitudes of applied magnetic fields than the ones we used for our device, and (3) the capability for remote operation (without the need for tether wires for power transmission and pump actuation), when combined with a wireless communication module, realizes a truly remotely activated drug delivery chip.

5.1.2.2 Magnetic Micro Mixer

A micromachined magnetic bar stirrer has been developed, and the basic schematic of the bar stirrer is shown in Figure 43. The micromagnetic bar is anchored by a hub. It is magnetized by an external magnetic field, and is capable of rotating under a remotely applied magnetic field. It was inspired by a macroscopic bar mixer.

Most microfluidic mixers are coupled with a flow channel, but not with a fluid reservoir or a reaction chamber. As a result, common biological procedures such as the mixing of two components are impossible. The magnetic bar mixer is motivated by the needs of biologist and chemists to have controlled mixing.

Currently a second-generation device is being developed. Although bar rotation has been demonstrated, smooth rotation has not been accomplished. The roughness of the mask contributes to this shortcoming. In the next generation device, the process and design will be optimized based on existing knowledge.

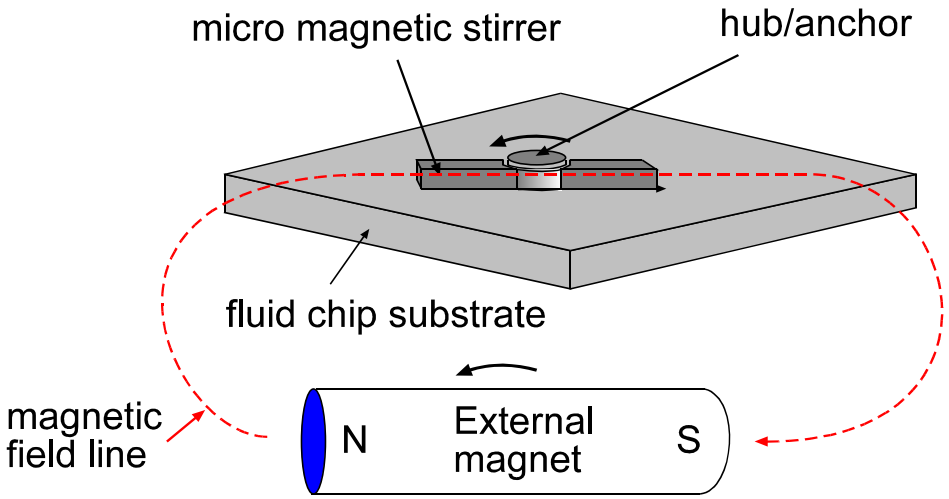

Figure 43. Schematic diagram of a micromachined micro mixer

In Figure 44 is presented a numerical simulation of the fluid flow forced by the moving magnetic bar in an effort to optimize the mixing performance. The simulation plot (Figure 45) illustrates tow fluids being mixed with a rotating magnetic bar stirrer.

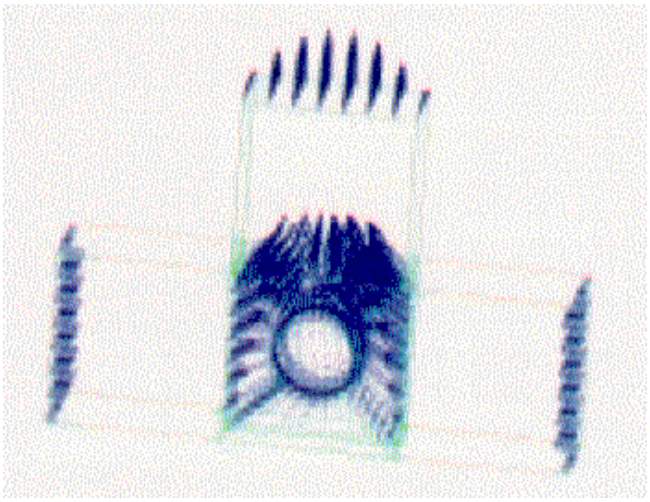

Figure 44. Illustration of two fluids being mixed with a rotating magnetic bar stirrer

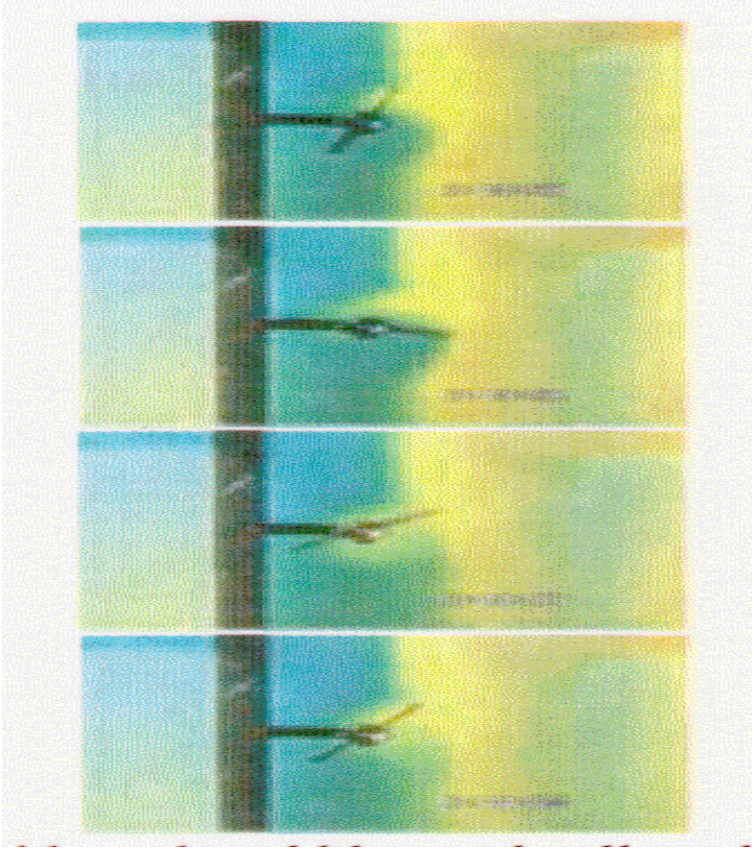

Figure 45. Sequential images of two fluids, colored blue and yellow, being mixed in a microchannel with a micro magnetic bar mixer

5.2 ELECTROKINETIC MICROCHANNEL GEOMETRIES

Electrokinetic microchannel geometries have been optimized, and novel flow diagnostics have been developed, and are discussed in this chapter.

5.2.1 Design and Optimization

A comprehensive effort to design and optimize electrokinetic turn geometries for minimally dispersive capillary electrophoretic separations was undertaken and completed. This analysis included the development of an analytical model and the implementation of novel diagnostic techniques to confirm the predictions from the analytical model. Two techniques, bleached fluorescence and caged fluorescence, were developed and applied as part of this Composite CAD project.

In Figure 46 is presented a caged fluorescence image of a flow field with both pressure driven and electroosmotic flow components. The band on the left is optically injected into the flow field using a 355 nm laser probe. The flow of the fluid is from left to right along the channel. On the right of this figure is the same band at a later time. The effect of the drag from the walls of the channel is evident from the shape of this band.

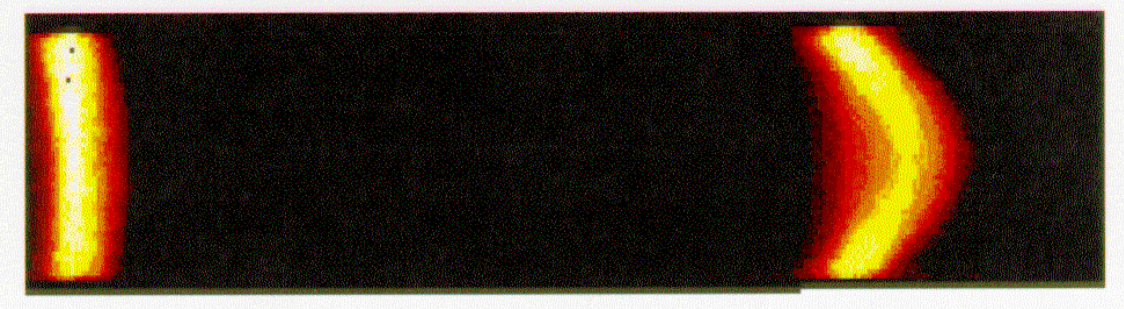

Figure 46. Caged fluorescence image of a flow field

The bleached fluorescence technique (29) was a novel technique with advantages that are very complimentary to those of caged fluorescence. Experimental results were compared with simulations to demonstrate that simulations could be used as effective design tools (Figure 47).

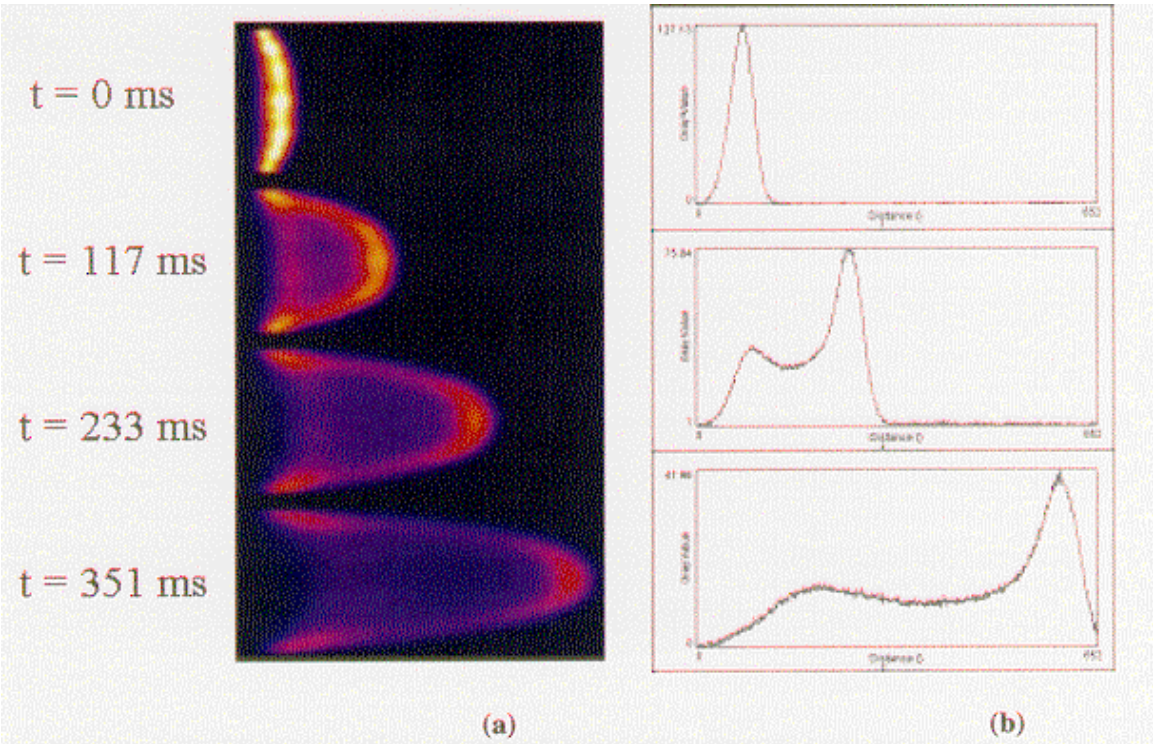

Figure 47. Imaging of the pressure driven flow in a microchannel using the improved caged fluorescence imaging system. The intensity of the plots shown in (b) correspond to the centerline of the first, second and forth images shown in (a).

In an initial study of the dispersion problem, an analytical model describing the dispersion caused by constant radius turns was developed. This model spanned the different regimes that exist for analyte dispersion in electrokinetic channels in the context of the advective-diffusion equation: axial diffusion limit, Taylor-Aris limit and the pure advection limit. Figure 48 shows the turn variance ratio as a function of the turn transport ratio for an 180º constant radius turn. The introduction of the non-dimensional term, t_{turn} allows for a quantitative determination of the dispersion regimes associated with the constant radius turn.

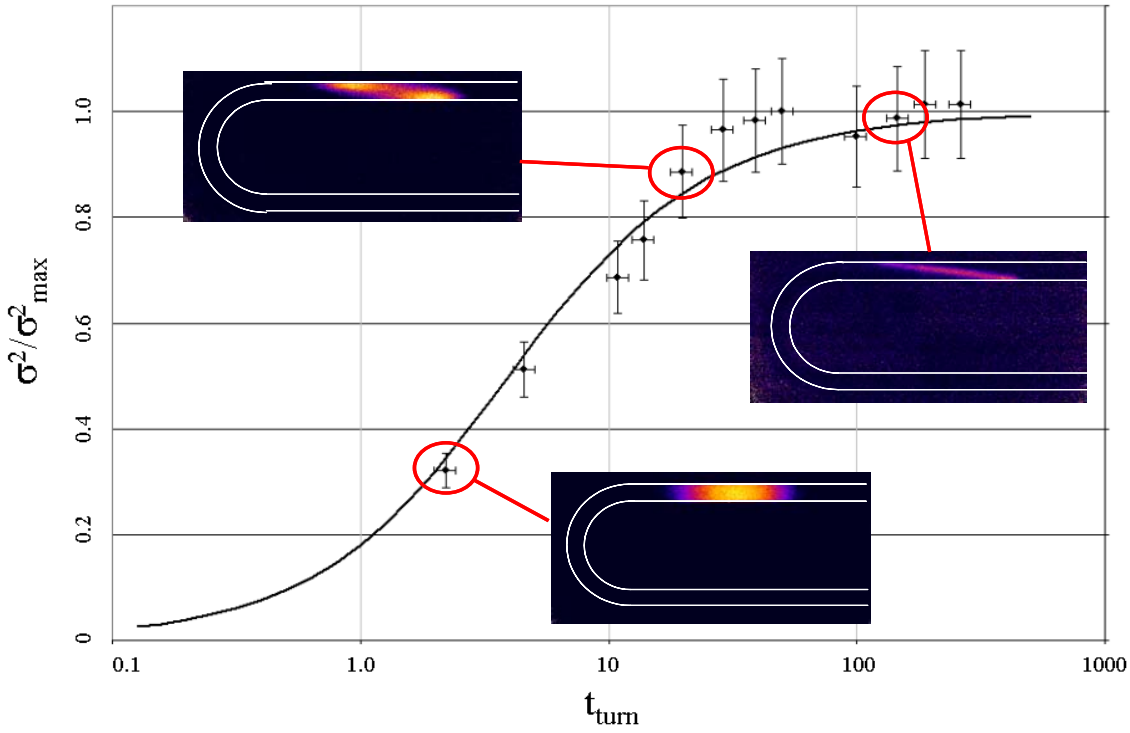

Figure 48. Turn variance ratio verses transport ratio for a 180º constant radius turn. The caged fluorescence images show the experimentally observed dispersion regimes for the different turn ratios

A novel technique, bleached fluorescence visualization, for imaging microflows was developed at the Stanford Microfluidics Laboratory. This technique was demonstrated as a viable tool for measuring molecular diffusivities and electrokinetic mobilities in both glass and acrylic channels (Aclara BioSciences). Figure 49 shows the evolution of a photo-bleached line in a steady electroosmotic flow field. A time-sequence of column averaged axial intensity profiles with corresponding Gaussian fits is shown in Figure 50. This method was demonstrated to yield a simultaneous measurement of the electrophoretic mobility and diffusion coefficient of the fluorescein dye.

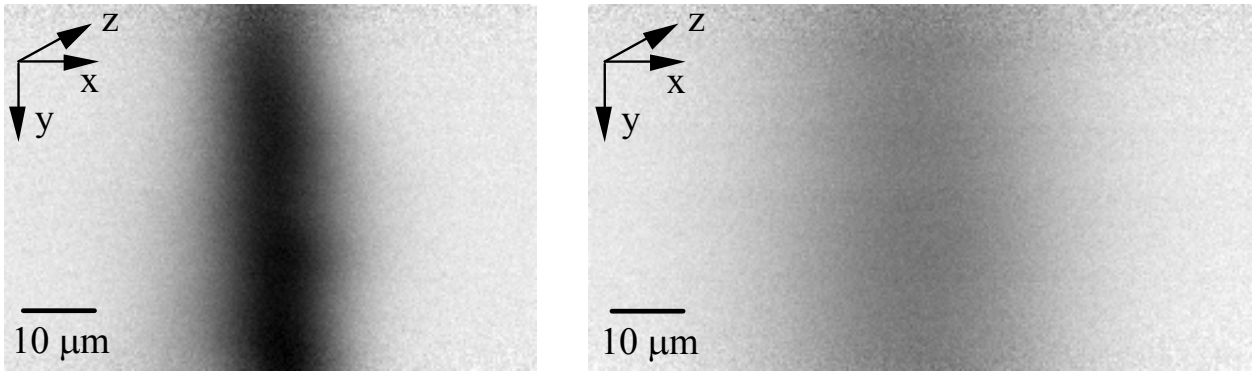

t = 0 s t = 0.53 s

Figure 49. Evolution of a photobleached line in steady electroosmotic flow field

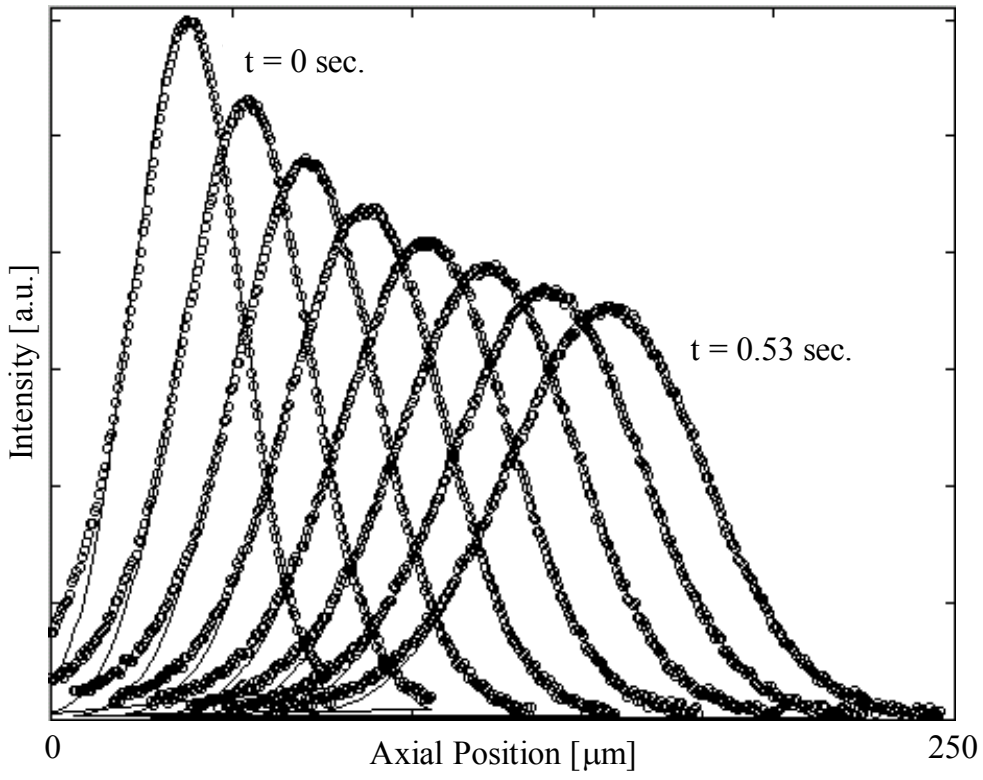

Figure 50. Time-sequence of column-averaged axial intensity profiles for the pure electroosmotic flow experiment shown in Figure 48

Both bleached and caged fluorescence techniques were applied to validate optimal electrokinetic turns for both 90º and 180º turns. Figure 51 shows the reduction in dispersion achieved through the optimized turn geometries compared to a simple 180º turn. A significant reduction in the variance has been shown for this particular geometry. The image with the optimized geometry displays a simultaneous separation of different specie present in the uncaged sample plug along with reduced sample dispersion.

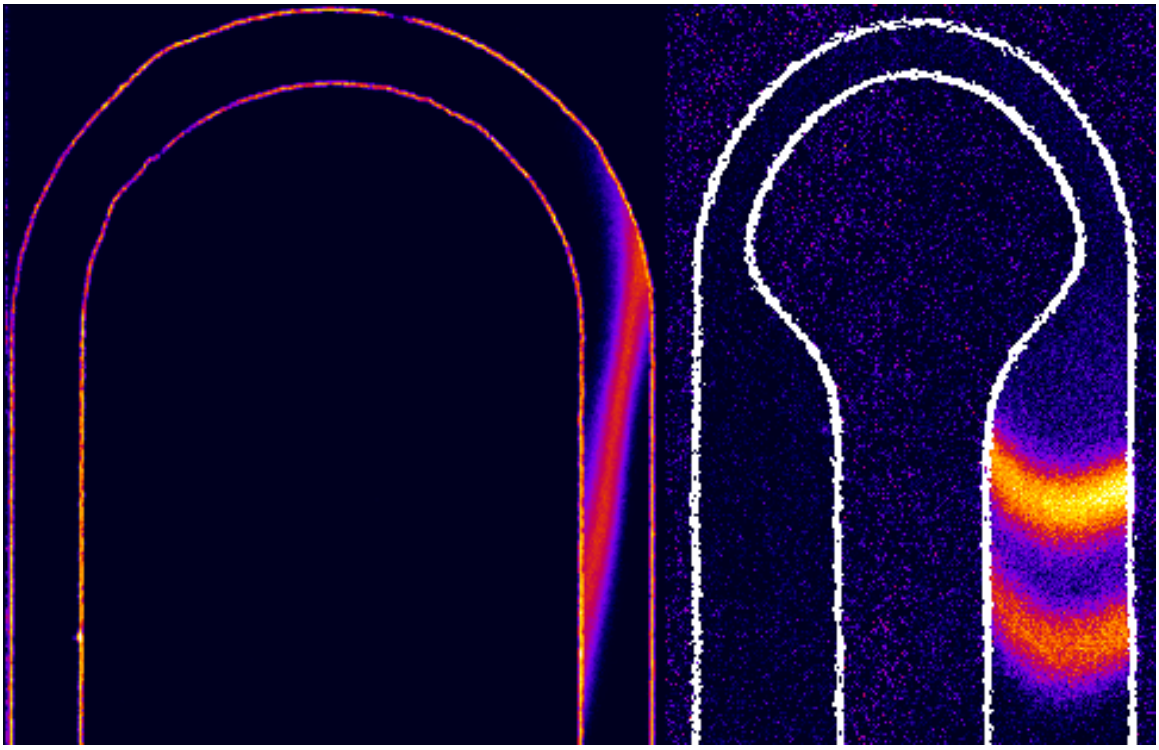

Figure 51. Caged fluorescence (i.e., experimentally obtained visualizations) results for dispersion of a sample plug around the two cases of a simple, uncorrected and a corrected 180º turn

5.2.2 Design Rules for Optimization

Design rules for the optimization of 90º and 180º constant radius turns have been proposed based on simulations and predictions from an analytical model developed. This model is valid across all the dispersive regimes allowed by the advective-diffusion

equation. A novel experimental technique, bleached fluorescence visualization, was implemented to verify these predictions (Figure 52). We also implemented caged-fluorescence visualization in these experiments and compared the two techniques. An optimized turn geometry shown to reduce the dispersion variance to less than 1% of a simple turn was proposed (Figure 53).

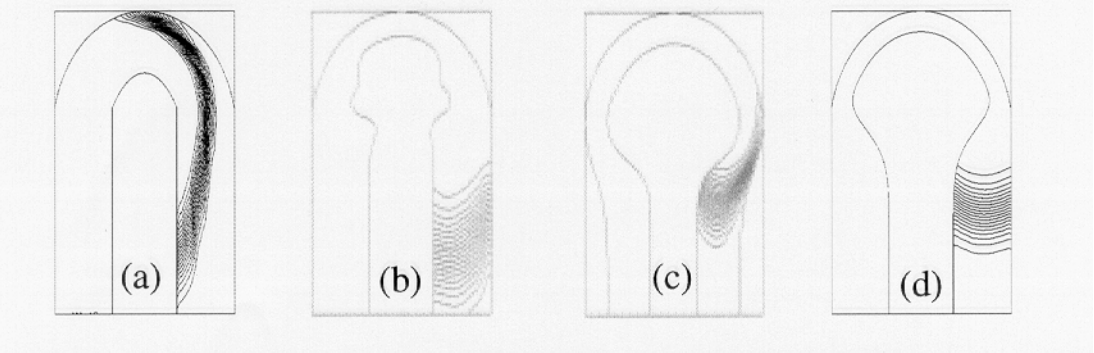

Figure 52. Simulations of microfluid flow in 180 degrees microchannel bends

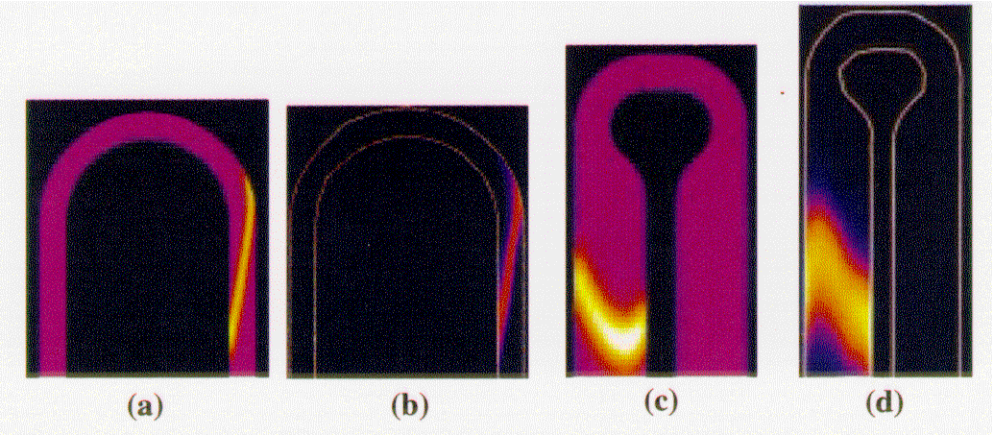

Figure 53. Caged fluorescence measurements of flows in 180 degree microchannel bends with different geometries

6. CONCLUSIONS

This project led to several breakthrough advances in computational prototyping tools for microfluidics. Sophisticated and advanced computational design tools were developed for microfluidics. These tools are several orders of magnitude faster than existing simulation tools. In addition, the radically new algorithms developed as part of this project have laid foundations for next generation design tools in microfluidics. All the design tools have been rigorously validated with experimental data. Using the design tools, several complex fluidic devices have been designed and several fabrication cycles have been eliminated through the use of these design tools. The results of this effort are being transitioned to commercial MEMS CAD companies, and some of this work is already embedded into their tools.

7. REFERENCES

1. N. R. Aluru, "CAD enabled MEMS innovation", *Journal of Materials Processing & Manufacturing Science*, Vol. 8, No. 4, pp. 325-327, April 2001.
2. D. Liu, M. Maxey and G.E. Karniadakis, A fast algorithm for particulate microflows in complex geometries Proc. ASME Winter Meeting, NY, November 2001.
3. I. Lomtev, R.M. Kirby, and G.E. Karniadakis, ``A discontinuous Galerkin ALE method for compressible viscous flows in moving domains", J. Comp. Phys., vol. 155, pp. 128-159, 1999.
4. C. Evangelinos, D. Lucor, C.-H. Su and G.E. Karniadakis, Flow-induced vibrations of non-linear cables, Part I: Models and algorithms, Int. J. Num. Meth. Engineering, to appear, 2001.
5. D. Lucor, C. Evangelinos, L. Imas and G.E. Karniadakis Flow-induced vibrations of non-linear cables, Part II: Simulations Int. J. Num. Meth. Engineering, to appear, 2001.
6. N. R. Aluru, "A point collocation method based on reproducing kernel approximations", *International Journal for Numerical Methods in Engineering,* Vol. 47, No. 6, pp. 1083-1121, 2000.
7. M. Mitchell, R. Qiao, and N. R. Aluru, "Meshless analysis of steady-state electroosmotic transport", *Journal of Microelectromechanical Systems, Vol. 9, No. 4, pp. 435-449, 2000*.
8. N. R. Aluru, "A reproducing kernel particle method for meshless analysis of microelectromechanical systems", *Computational Mechanics*, Vol. 23, No. 4, pp. 324-338, 1999.
9. N. R. Aluru and G. Li, "Finite Cloud Method: A true meshless technique based on a fixed reproducing kernel approximation", *International Journal for Numerical Methods in Engineering, Vol. 50, No. 10, pp. 2373-2410, 2001*.
10. R. Ohs and N. R. Aluru, "Meshless analysis of piezoelectric devices", *Computational Mechanics, Vol. 27, No. 1, pp. 23-36, 2001.*
11. G. Li and N. R. Aluru, "Boundary Cloud Method: A combined scattered point/boundary- integral approach for boundary-only analysis", *Accepted for Publication in Computer Methods in Applied Mechanics and Engineering*, 2001.
12. Vaishali Shrivastava and N. R. Aluru, "A fast boundary cloud method for exterior 2-D electrostatic analysis", *Submitted for Publication*, 2001.
13. Gang Li and N. R. Aluru, "Linear, nonlinear and mixed-regime analysis of electrostatic MEMS", *Sensors and Actuators A*, Vol. 91, No. 3, pp. 278-291, 2001.

14. O. Aktas, N. R. Aluru, U. Ravaioli, “Application of a parallel DSMC technique to predict flow characteristics in microfluidic filters” *Journal of Microelectromechanical Systems*, Vol. 10, No. 4, pp. 538-549, 2001.
15. O. Aktas and N. R. Aluru, “A combined continuum/DSMC approach for multiscale analysis of microfluidic filters”, *Submitted for Publication*, 2001.
16. R.M. Kirby, G.E. Karniadakis, O. Mikulchenko, K. Mayaram An Integrated Simulator for Coupled Domain Problems in MEMS, J. MEMS, vol. 10 (3), p. 379, 2001.
17. R.M. Kirby, G.E. Karniadakis, O. Mikulchenko, K. Mayaram Integrated Simulation for MEMS: Coupling Flow-Structure-Thermal-Electrical Domains, Chapter 5, The MEMS Handbook, edited by M. Gad-el-Hak, CRC, 2001.
18. Deniz Armani, Chang Liu**,** "Re-configurable Fluid Circuits By PDMS Elastomer Micromachining"**,** 12th International Conference on MEMS, MEMS 99, pp.222-227, Orlando, FL, 1998.
19. X. Wang, L.H. Lu, C. Liu, *"Micromachining Techniques for Liquid Crystal Polymer",* MEMS 01, Switzerland, January 2001.
20. L.H. Lu, X. Wang, C. Liu, *"An efficient low-cost micro fabrication method of capillary electrophoresis chip using liquid crystal polymer (LCP)",* L1006, 14th International Symposium on Microscale Separations and Analysis, January 13-18, 2001, Boston, MA.
21. J.I. Molho, AE Herr, BP Mosier, JG Santiago, TW Kenny, et al., “*A low dispersion turn for miniaturized electrophoresis”,* Solid State Sensor and Actuator Workshop, Hilton Head Island, SC. 2000.
22. Bo Choi, Min Ma, Christopher White, Chang Liu, "Electrolytic and thermal bubble generation using AC inductive powering," International Conference on Solid-State Sensors and Actuators (Transducer'99), Sendai, Japan, 7-10 June 1999.
23. D. Armani, C. Liu, *"Microfabrication Technology for Polycaprolactone, A Biodegradable Polymer"*, J. of Micromechanics and Microengineering, 10, pp. 80-84, 2000.
24. D. Armani, C. Liu, *"Microfabrication Technology for Polycaprolactone, A Biodegradable Polymer"* Int. Conf. on MEMS, MEMS 2000, Japan.
25. M. Khoo, C. Liu, *"Micro magnetic silicone elastomer membrane actuator, "* Sensors and Actuators, vol. 89, no. 3, pp. 259-266, March, 2001.
26. Chang Liu, *"A magnetic flexible membrane actuator for micro fluid pumping (Invited)",* Sixth International Symposium on Magnetic Materials, Processes and Devices, a Symposium at the 198th Meeting of the Electrochemical Society, Oct 22-27, 2000, Phoenix, Arizona.

27. Melvin Khoo, C. Liu, *"Development of A Novel Micromachined Magnetostatic Membrane Actuator",* The 58th Annual IEEE Device Research Conference, pp. 109-110, Denver, CO, 2000.

28. Melvin Khoo, C. Liu, *"A Novel Micromachined Magnetic Membrane Microfluid Pump"***,** 22nd Annual International Conference of the IEEE Engineering in Medicine and Biology Society, 2000, Chicago, IL.

29. BP Mosier, JI Molho and JG Santiago, Experiments in Fluids, submitted 2001.

30. D. Liu, M. Maxey and G.E. Karniadakis, A fast algorithm for particulate microflows in complex geometries Proc. ASME Winter Meeting, NY, November 2001.

31. G. Li and N. R. Aluru, "A Lagrangian approach for electrostatic analysis of deformable conductors", *Accepted for Publication in Journal of Microelectromechanical Systems*, 2001.

32. L-H Lu, K. Ryu, C. Liu, *"A Novel Microstirrer and Arrays for Microfluidic Mixing,"* Fifth International Conference on Miniaturized Chemical and Biochemical Analysis Systems, Oct 21-25, 2001.

APPENDIX I. SYMBOLS, ABBREVIATIONS AND ACRONYMS

MEMS	MicroElectro Mechanical Systems
SPICE3	A general purpose circuit simulator
Νεκταr	A general purpose CFD code for simulating incompressible, compressible and plasma flows in unsteady three-dimensional geometries
DSMC	Direct Simulation Monte Carlo method for fluidic flows through narrow channels
FASTSTOKES	Precorrected-FFT accelerated Stokes flow solver.
CAD	Computer Aided Design
EOFLOW	
FFT	Fast Fourier Transform
FASTWAMIT	Fast analysis program for offshore structure analysis
MIT	Massachusetts Institute of Technology
t_{spice}	Time for membrane actuation
t_{call}	Time for the next call
MEMS	MicroElectro Mechanical Systems
V	Voltage
Vout	Output Voltage
Rn	Resistance value of n
Tn	Solution at n
Tsso	Steady state solution of neural network
P	Pressure
U	Flow velocity
SEM	Scanning electron Microscope
Q	Flowrate
$\underline{\chi}$	Heat Source
LCP	Liquid Crystal Polymer
CFD	Computation Fluid Dynamics
LCP	Liquid crystal polymer